Mechanical Systems and Signal Processing 79 (2016) 225–253

Contents lists available at ScienceDirect

Mechanical Systems and Signal Processing

journal homepage: www.elsevier.com/locate/ymssp

Chaotic dynamics of flexible beams driven by external white noise

J. Awrejcewicz [a,b,*], A.V. Krysko [c,d], I.V. Papkova [e], V.M. Zakharov [e], N.P. Erofeev [e], E.Yu. Krylova [e], J. Mrozowski [a], V.A. Krysko [e]

[a] Department of Automation, Biomechanics and Mechatronics, Lodz University of Technology, 1/15 Stefanowski St., 90-924 Lodz, Poland
[b] Institute of Vehicles, Warsaw University of Technology, 84 Narbutta Str., 02-524 Warsaw, Poland
[c] Department of Applied Mathematics and Systems Analysis, Saratov State Technical University, 77 Politehnicheskaya Str., 41054 Saratov, Russian Federation
[d] Cybernetic Institute, National Research Tomsk Polytechnic University, 30 Lenin Avenue, 634050 Tomsk, Russian Federation
[e] Department of Mathematics and Modeling, Saratov State Technical University, 77 Politehnicheskaya Str., 410054 Saratov, Russian Federation

ARTICLE INFO

Article history:
Received 19 February 2016
Accepted 23 February 2016
Available online 29 March 2016

Keywords:
Parametric vibrations
Noise-induced transitions
Beams
Fourier and wavelet analysis

ABSTRACT

Mathematical models of continuous structural members (beams, plates and shells) subjected to an external additive white noise are studied. The structural members are considered as systems with infinite number of degrees of freedom. We show that in mechanical structural systems external noise can not only lead to quantitative changes in the system dynamics (that is obvious), but also cause the qualitative, and sometimes surprising changes in the vibration regimes. Furthermore, we show that scenarios of the transition from regular to chaotic regimes quantified by Fast Fourier Transform (FFT) can lead to erroneous conclusions, and a support of the wavelet analysis is needed. We have detected and illustrated the modifications of classical three scenarios of transition from regular vibrations to deterministic chaos. The carried out numerical experiment shows that the white noise lowers the threshold for transition into spatio-temporal chaotic dynamics. A transition into chaos via the proposed modified scenarios developed in this work is sensitive to small noise and significantly reduces occurrence of periodic vibrations. Increase of noise intensity yields decrease of the duration of the laminar signal range, i.e., time between two successive turbulent bursts decreases. Scenario of transition into chaos of the studied mechanical structures essentially depends on the control parameters, and it can be different in different zones of the constructed charts (control parameter planes). Furthermore, we found an interesting phenomenon, when increase of the noise intensity yields surprisingly the vibrational characteristics with a lack of noisy effect (chaos is destroyed by noise and windows of periodicity appear).

* Corresponding author.
E-mail addresses: awrejcew@p.lodz.pl (J. Awrejcewicz), anton.krysko@gmail.com (A.V. Krysko), ikravzova@mail.ru (I.V. Papkova), zakharov.victor@gmail.com (V.M. Zakharov), erofeevnp@mail.ru (N.P. Erofeev), Kat.Krylova@bk.ru (E.Yu. Krylova), jerzy.mrozowski@p.lodz.pl (J. Mrozowski), tak@san.ru (V.A. Krysko).

http://dx.doi.org/10.1016/j.ymssp.2016.02.043
0888-3270/

1. Introduction

It is well known that in deterministic physical systems there are several scenarios of transition from regular to chaotic oscillations. Ruelle and Takens [1] have shown that chaos can be achieved via combination of only three frequencies. "Noisy" behavior in this scenario is associated with a strange attractor arisen after three consecutive Hopf bifurcations [2]. Simple deterministic systems are able to generate internal chaotic response. It can be realized via a sequence of Hopf bifurcations, and the period doubling scenario through intermittency [2–4]. On the other hand, a random nature of the input may induce much richer variety of non-linear phenomena than those regarding purely deterministic cases. It is expected that noisy transitions from regular to chaotic dynamics exhibited by structural members are similar to the phase transitions, and to the transitions occurring in non-equilibrium systems with deterministic external inputs. We are aimed to show that it is possible to extend the classical transition scenarios and associated non-linear phenomena to physical systems in which the noise plays an important role. Thus, it becomes possible to carry out the theoretical study of noisy induced transitions into chaotic regimes of the studied continuous mechanical systems. Theory of deterministic multidimensional systems has been already introduced in references [5–15]. The present work aims to apply and extend these studies in the event of noise-induced transitions.

Though a study of chaotic vibrations of structural systems attracted a large attention within community of applied mathematicians and engineers usually, the problem has been strongly reduced to that of non-linear dynamics of either one- or two-degrees-of-freedom lumped systems. For example, fluctuations in distributed systems are often replaced by a study of the single-mode non-linear vibrations of Bernoulli–Euler beams, taking into account the geometric nonlinearity. The results of these studies should be considered as qualitative, since the increase in the number of modes often leads to substantially different non-linear dynamics. In reference [16] global bifurcations and chaotic dynamics in nonlinear plane vibrations of a cantilever beam under axial harmonic excitation and transverse excitations at the free end of the beam are studied. Finite element method for the study of forced nonlinear oscillations of the beam has been applied in work [17]. Chaos exhibited by vibrations of plates and shells with geometric nonlinearities has been extensively analyzed in references [5–13]. In the case of beams, the new stochastic linearization method has been applied to investigate the non-linear mean square response of a beam under time-dependent stationary random excitation [18]. It has been shown, that the proposed technique can yield more accurate results for the mean square response of the beam in comparison to the standard stochastic linearization approach. Dahlberg [19] has applied the model analysis to study the influence of modal cross-spectral densities versus the spectral densities of simply supported beams. The response power spectral density and mean-square response have been used by Jacquot [20] while studying beam structures excited by a stationary random process. The effect of axial loads on transverse vibrations of an Euler–Bernoulli clamped-pinned beam under random vibration has been analyzed in reference [21]. The concepts of the moment Lyapunov exponent and the Lyapunov exponent of a Timoshenko beam under bounded noise excitation have been used in reference [22]. Both almost-sure stability and moment stability of the stationary solutions of the elastic beam subjected to the stochastic axial load have been investigated. The so called shape memory alloy beams non-linear dynamics have been studied including bifurcation and chaotic phenomena [23–25]. The superelastic shape memory alloy systems under random stationary excitations have been analyzed in reference [26]. Recently, the shape memory alloy beam under narrow band noise excitations (harmonic function with constant amplitude and random frequency) has been investigated by Ge [27]. However, a strong Galerkin-based truncation of the governing PDEs reduced the consideration to non-linear one-degree-of freedom mechanical systems. The electromechanical response of the pre-buckled inverted cantilevered beam subjected to a combination of harmonic and broadband random excitation has been studied by Friswell et al. [28]. Since the pre-buckled beam stiffness is low, the displacement response yielded multiple solutions being exploited in the harvesting device. The amplitude of random noise excitation, where the harvester is unable to sustain the high amplitude solution, has been investigated and validated experimentally.

In the case of plates, active control of noise radiation from vibrating plate excited by a harmonic line moment has been proposed by Lee and Chen [29]. The control has been achieved by various configurations of piezoelectric actuators and the optimal control unit voltage has been utilized. It has been shown, among other, that the model suppression and modal restructuring play a key role in radiated power attenuation. Numerical prediction of noise transmission loss through sandwich plates subjected to an acoustic plane wave or a diffuse sound field excitation has been reported by Assaf and Guerich [30]. The diffuse sound field has been modeled as a superposition of uncorrelated plane waves with equal amplitude, whereas the vibroacoustic equations have been discretized by a triangular finite element. A stochastic non-linear model has been proposed to describe vibrations of a rectangular thin plate under axial inplane excitation with random environment factors, and the stochastic Hopf bifurcation of the vibration model has been investigated [31]. Wiciak [32] has investigated reduction of plate vibrations and radiated noise by using piezoelectric actuators in an asymmetric configuration. In particular, influence of the actuators activation and shape form on the plate response has been studied, and the experimental results have been compared with the numerical approach based on the finite element method. Both motion and sound of a thin elastic plate subjected to uniform low-Mach flow and actuated at its leading edge, has been studied by Manela [33]. Periodic and non-periodic actuations have been investigated.

In the case of shells we report only a few works. White [34] investigated the transmission of an acoustic wave through an infinite, nonhomogeneous closed cylindrical shell. It has been shown that the presence of stiffening corrugations and irregularities in the shell leads to a random-vibration field, and hence the transmission of random sound through flat panels can be used for noise-reduction estimates. Durant et al. [35] established a comparison between the measured and the

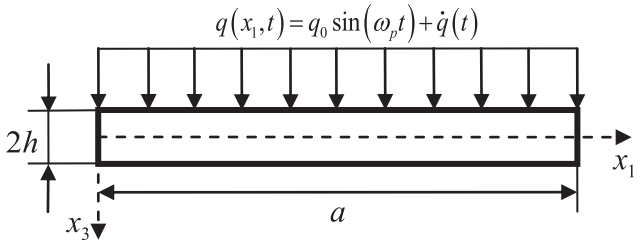

Fig. 1. Scheme of the investigated beam.

modeled vibroacoustic response of a thin cylindrical pipe excited by a turbulent internal flow. In spite of the experimental investigation, the paper offers a numerical technique based on a boundary integral formulation and a matched asymptotic expansion. Experimental and theoretical analysis of circular cylindrical shells under seismic-like base excitation has been carried out by Pellicano [36]. The developed model takes into account geometric shell nonlinearities, electrodynamic shaker equations and the shell shaker interaction.

The paper is organized in the following way. In Section 2 mathematical models of flexible beams are introduced, the non-dimensional PDEs are given, and the numerical analysis of the system of non-linear ODEs has been carried out. The similar like study has been reported in Section 3, where two non-linear PDEs governing flexible rectangular plate dynamics have been analyzed. Section 4 reports bifurcational and chaotic dynamics of spherical shells using polar coordinates, whereas Section 5 summarizes the obtained results.

2. Beam model

The object of our study is a single-layer beam which occupies a two-dimensional region of space R^2 with a Cartesian coordinate system $Ox_1x_2x_3$ introduced in the following way: axis Ox_1 is directed from left to right along the beam midline, whereas axis Ox_3 is directed downward and is perpendicular to axis Ox_1 (see Fig. 1). In the introduced system of coordinates, the beam two-dimensional domain Ω is defined as follows: $\Omega=\{x_1\in[0,a];\ -h\le x_3\le h\}$, $0\le t\le\infty$. Here and below we use the following notation: $2h$ denotes the beam height, and a is the length of the beam.

The mathematical model of the beam is based on Bernoulli–Euler's hypothesis which takes into account the non-linear relationship between stresses and strains in the Kármán form [37]. The system of differential equations regarding displacements and governing the beam motion, including dissipation effect, is as follows [38]:

$$\begin{aligned}
&E\left\{\frac{\partial^2 u}{\partial x_1^2}+L_3(w,w)\right\}-\frac{\gamma}{g}\frac{\partial^2 u}{\partial t^2}=0,\\
&E\left\{L_1(u,w)+L_2(w,w)-\frac{(2h)^2}{12}\frac{\partial^4 w}{\partial x_1^4}+q+\dot{q}\right\}-\frac{\gamma}{g}\frac{\partial^2 w}{\partial t^2}-\varepsilon\frac{\gamma}{g}\frac{\partial w}{\partial t}=0,\\
&L_1(u,w)=\frac{\partial^2 u}{\partial x_1^2}\frac{\partial w}{\partial x_1}+\frac{\partial u}{\partial x_1}\frac{\partial^2 w}{\partial x_1^2},\ L_2(w,w)=\frac{3}{2}\frac{\partial^2 w}{\partial x_1^2}\left(\frac{\partial w}{\partial x_1}\right)^2,\ L_3(w,w)=\frac{\partial^2 w}{\partial x_1^2}\frac{\partial w}{\partial x_1}.
\end{aligned}\tag{1}$$

We have applied the following notation: $w(x_1,t)$ – beam deflection; $u(x_1,t)$ – beam movement along the axis Ox_1; ε – dissipation coefficient; $q=q(x_1,t)$ – transverse load; $\dot{q}(t)$ – white noise generated by the function $w_n\cdot(2.0\cdot\mathrm{rand}()/(\mathrm{RAND\_MAX}+1.0)\text{-}1.0)$, E – Young's modulus, γ – volume weight of beam material; g – acceleration of gravity. We introduce the following dimensionless variables

$$\overline{w}=\frac{w}{2h},\quad \overline{u}=\frac{ua}{(2h)^2},\quad \overline{x}_1=\frac{x_1}{a},\quad \lambda=\frac{a}{2h},\quad \overline{q}=q\frac{a^4}{(2h)^4E},\quad \overline{t}=\frac{t}{\tau},\quad \tau=\frac{a}{c},\quad c=\sqrt{\frac{Eg}{\gamma}},\quad \overline{\varepsilon}=\varepsilon\frac{a}{c},\tag{2}$$

and two partial differential equations called further PDEs (1) governing dynamics of the beam are given in the following non-dimensional counterpart form:

$$\begin{aligned}
&\frac{\partial^2 u}{\partial x_1^2}+L_3(w,w)-\frac{\partial^2 u}{\partial t^2}=0,\\
&\frac{1}{\lambda^2}\left\{L_2(w,w)+L_1(u,w)-\frac{1}{12}\frac{\partial^4 w}{\partial x_1^4}+q+\dot{q}\right\}-\frac{\partial^2 w}{\partial t^2}-\varepsilon\frac{\partial w}{\partial t}=0,
\end{aligned}\tag{3}$$

where dashes above the dimensionless parameters are omitted for simplicity. The following boundary conditions are introduced

$$w(0,t)=w(1,t)=u(0,t)=u(1,t)=\partial^2 w(0,t)/\partial x_1^2=\partial^2 w(1,t)/\partial x_1^2=0.\tag{4}$$

We also apply the following initial conditions

$$w(x_1,t)|_{t=0}=\frac{\partial w(x_1,t)}{\partial t}|_{t=0}=u(x_1,t)|_{t=0}=\frac{\partial u(x_1,t)}{\partial t}|_{t=0}=0. \tag{5}$$

3. Method of solution of PDEs

In what follows we replace differential operators in space variable x_1 by difference operators for functions $w(x_1,t)$, $u(x_1,t)$ with the help of FDM (Finite Difference Method) with approximation $O\left(\Delta^2\right)$. Difference operators in approximation $O(\Delta^2)$, where Δc denotes the step along the spatial coordinate, are as follows: $\Lambda_{x_1}(\cdot_i)=\left((\cdot)_{i+1}-(\cdot)_{i-1}\right)/2\Delta$, $\Lambda_{x_1^2}(\cdot_i)=\left((\cdot)_{i+1}-2(\cdot)_i+(\cdot)_{i-1}\right)/\Delta^2$, $\Lambda_{x_1^4}(\cdot_i)=\left((\cdot)_{i+2}-(\cdot)_{i+1}+6(\cdot)_i-(\cdot)_{i-1}+(\cdot)_{i-2}\right)/\Delta^4$.

Therefore, partial differential Eq. (3) are reduced to the following ordinary differential equations (ODEs) of the second order regarding the time coordinate:

$$\begin{aligned}&\ddot{u}_\tau=\Lambda_{x_1^2}(u_i)+\Lambda_{x_1}(w_i)\Lambda_{x_1^2}(w_i),\\&\ddot{w}_t+\varepsilon\dot{w}_t=\tfrac{1}{\lambda^2}\Big\{-\tfrac{1}{12}\Lambda_{x_1^4}(w_i)+\Lambda_{x_1^2}(u_i)\Lambda_{x_1}(w_i)+\Lambda_{x_1^2}(w_i)\Lambda_{x_1}(u_i)+\tfrac{3}{2}\left(\Lambda_{x_1}(w_i)\right)^2\Lambda_{x_1^2}(w_i)+q+\dot{q}\Big\}.\end{aligned} \tag{6}$$

The obtained system of the second order ODEs (6) with appropriate boundary (4) and initial (5) conditions, yielded by the second order finite-difference approximation, is then reduced to a system of ordinary first order differential equations. The latter is solved by the 4th order Runge-Kutta method. In references [39–41] a few ben order Runge-Kutta method instead of 6th order Runge-Kutta method while solving the Cauchy problem have been discussed. Since numerical results obtained by the two mentioned methods are identical, preference is given to the 4th order Runge–Kutta method which requires less computational time in comparison to the 6th order Rungeutta method.

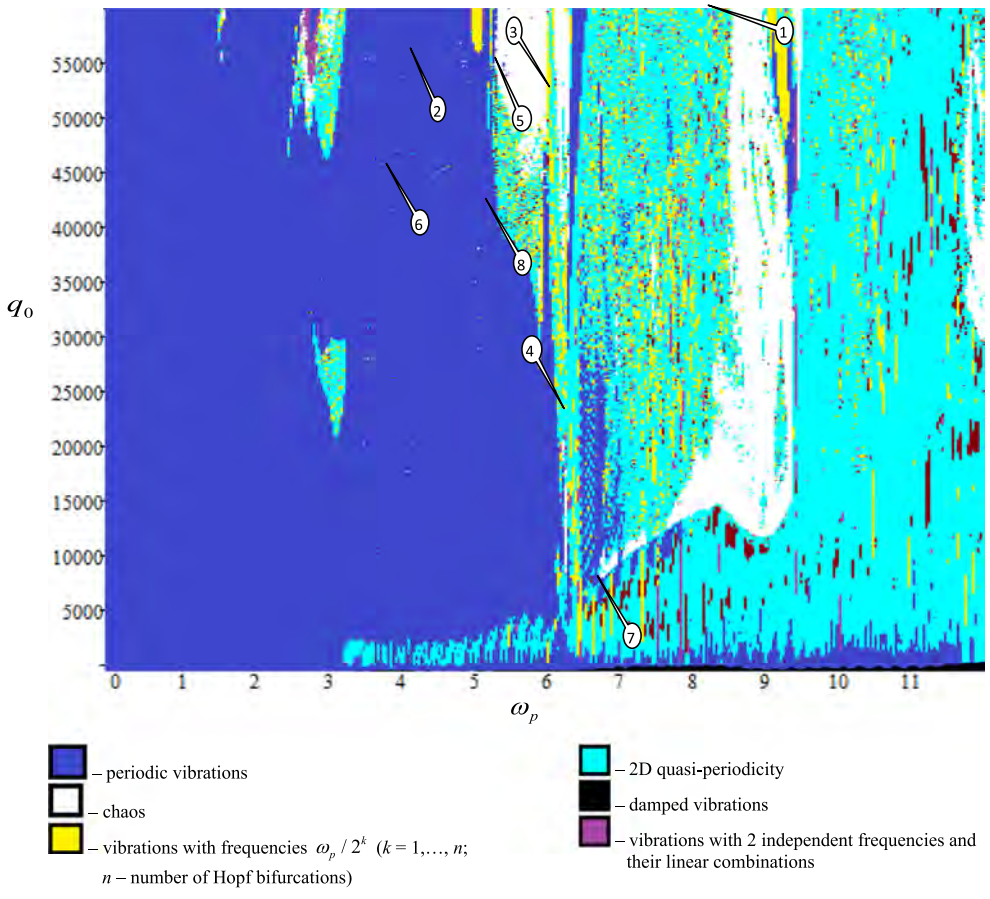

Fig. 2. Chart of the beam vibrations type: $w_n=0$, $\omega_p\in(0.0003;\ 12)$, $q_0\in(100;\ 60000)$.

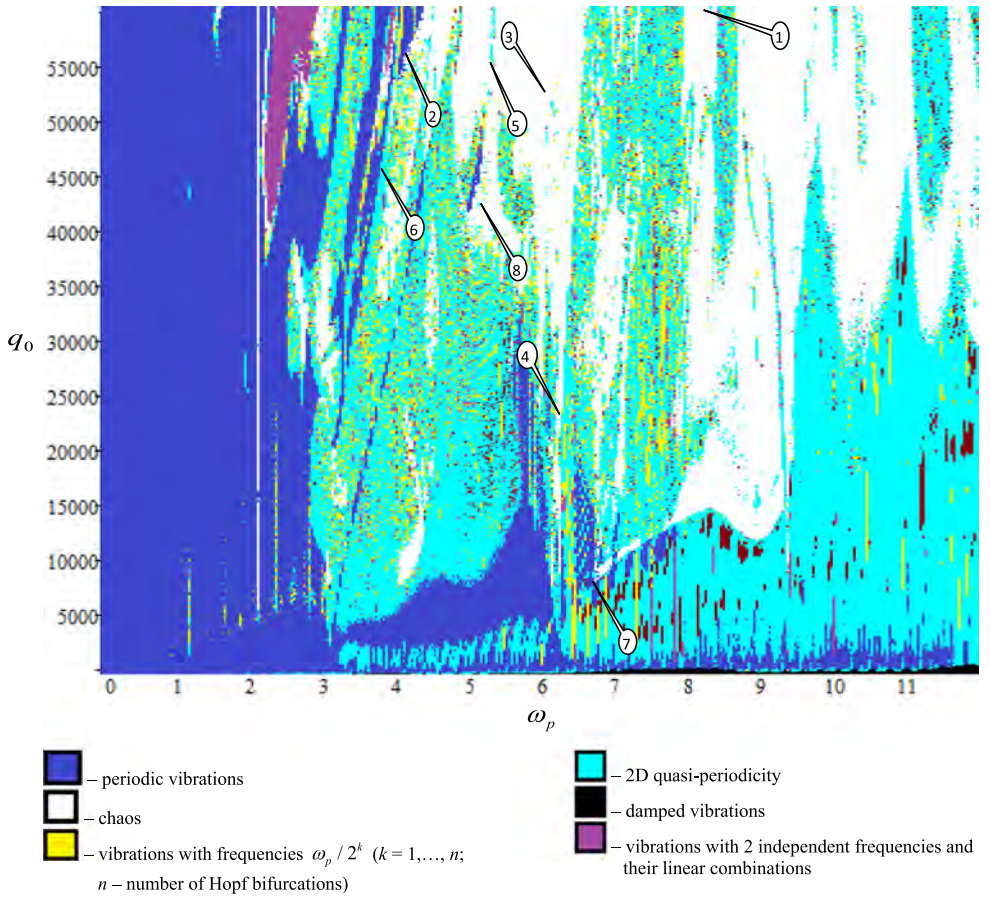

Fig. 3. Chart of the beam vibrations type: $w_n = 0.01$, $\omega_p \in (0.0003; 12)$, $q_0 \in (100; 60000)$.

4. Numerical analysis

In order to study dynamic behavior of nonlinear beams under the action of harmonic lateral load $q = q_0 \sin(\omega_p t)$, we have used a software package focused on a study of vibrations of beams as a function of the control parameters $\{q_0, \omega_p, w_n\}$. The developed algorithm allows us to detect and locate the zones of periodic vibrations, period doubling bifurcation zones, quasi-periodic zones as well as the zones of chaos. In order to get further reported charts of the beam vibration regimes, time histories of beam deflection $w(t)$ in the middle of the beam, where $x_1 \in [0;\ 1]$ interval is divided into 40 parts, have been studied (not reported here). The time history/signal is computed over time interval $t \in [0;\ 1024]$ for boundary conditions (4) and it may exhibit either regular or chaotic vibrations of the system (data concerning the type of vibrations are presented in Figs. 2–4). It is worth mentioning that to get maps/charts of the beam vibration regime versus two control parameters: $q_0 \in [100; 60000]$ (mesh consisting of 600 parts) and for $\omega_p \in [0.0003;\ 12]$ (mesh consisting of 350 parts) it is necessary to analyze $2.1 \cdot 10^5$ variants of the solution of the derived mathematical model. Each variant is accompanied by a study of the signals, power spectra constructed using FFT, Morlet wavelets, phase and modal portraits, autocorrelation functions, as well as signs of maximum Lyapunov exponents (to identify the kind of non-linear dynamics). The Lyapunov exponents are calculated by the method of neural networks [42] and the method proposed by Wolf [43]. The vibration regimes including periodic and chaotic attractors, bifurcations, damped vibrations and undefined system states have been identified (further results are given only for fixed $\lambda = 50$). In Figs. 2–4 eight points are chosen: for $w_n = 0$ (the lack of white noise), and for two values of the amplitude of external noise $w_n = 0.01$ and $w_n = 1$. The overall analysis of the maps shows that the presence of even small noise magnitude significantly reduces the zones of periodic vibrations. However, an increase of the intensity of white noise yields a negligible effect on the change in the location of periodicity zones.

The coordinates of the mentioned eight points are shown in Figs. 2–4 and their further numerical analysis is conducted using two-dimensional spectra obtained via the Morlet wavelet, Fourier power spectra, phase 2D and 3D portraits, pseudo Poincaré maps, as well as by a few (up to four) Lyapunov exponents (they are not reported here). If four values of the Lyapunov exponents are given, they are obtained via neural networks procedure, whereas the largest Lyapunov exponent is estimated by the Wolf algorithm [43].

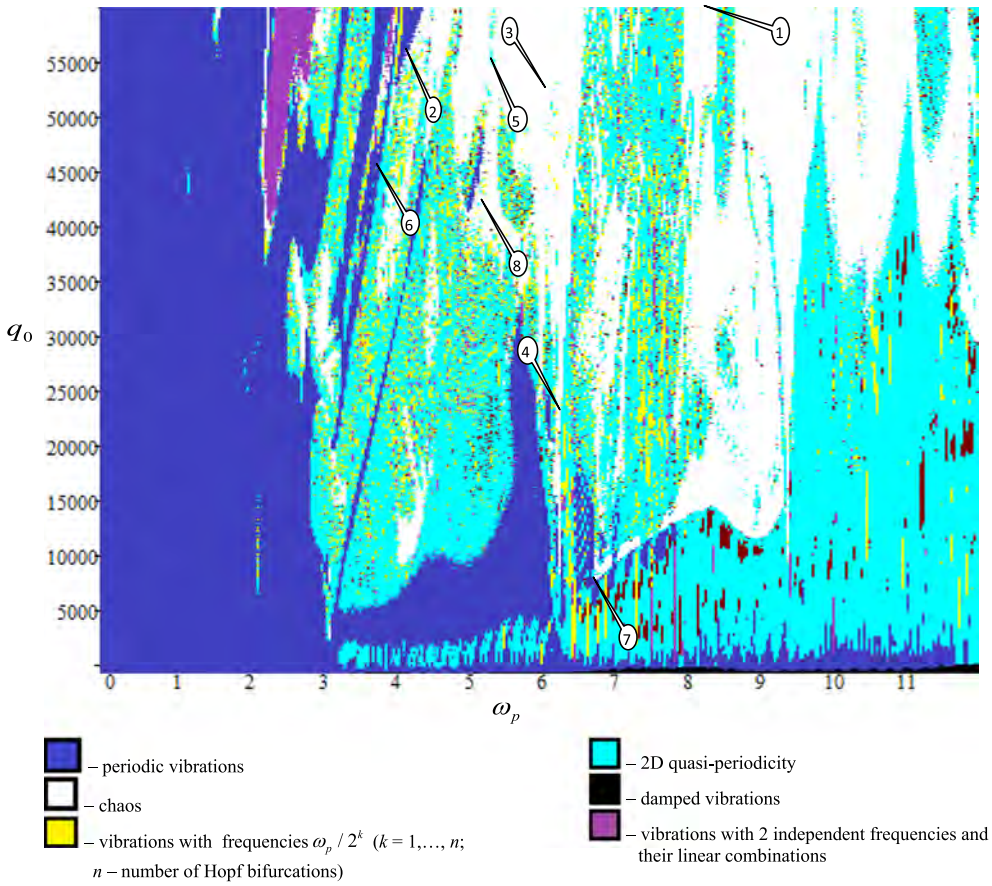

Fig. 4. Chart of the beam vibrations type: $w_n = 1$, $\omega_p \in (0.0003; 12)$, $q_0 \in (100; 60000)$.

At point 1 (Fig. 5) two-frequency oscillations (ω_1/ω_p is irrational number) and the presence of two Hopf bifurcations are observed (we have subharmonics $\omega_p/2$, $\omega_p/4$ and $\frac{3}{4}\omega_p$) for $w_n = 0$. White noise intensity of 0.01 shifts the system in the state of chaos spanned on the mentioned before frequencies. Increasing the intensity of external noise for the same external parameters ($w_n = 1$), we also get chaos spanned on the same frequencies, but chaotic vibrations vary significantly and "switch on" and "switch off" of the lower frequencies can be observed. In other words, the transition of the system into state of chaos is very sensitive to the applied noise intensity.

Point 2 (Fig. 6), in the absence of external noise, corresponds to almost harmonic vibrations with the frequency ω_p. The presence of external noise ($w_n = 0.01$) pushes the system into a subharmonic vibration regime via only one Hopf bifurcation. In addition, the system does not exhibit any sensitivity regarding low and high amplitude of the white noise action (increase of the noise intensity $w_n = 1$ does not change the subharmonic regime qualitatively). The Feigenbaum scenario yielding chaos via period doubling bifurcations has not been detected in this case, and surprisingly the frequency spectrum is smooth without any noisy components.

At point 3 (Fig. 7), in the absence of white noise, a slightly chaotic dynamics (LLE = 0.01819) and associated with five Hopf bifurcations is detected. Small presence of white noise pushes the system into chaotic state with the same fundamental frequencies, but with noisy components and more developed chaotization (LLE = 0.01405). The obtained chaotic attractor is robust, since we have not observed the qualitatively change while increasing w_n up to the value 1.0. At point 4 (Fig. 8), in the absence of noise the beam exhibits slightly developed quasi-periodic vibrations with two-frequencies ($\omega_1; \omega_p$), and a period three bifurcation is detected (occurrence of $\omega_p/3$). For $w_n = 0.01$ and $w_n = 1.0$, the beam vibrates chaotically with noisy frequency spectrum. Point 5 (Fig. 9) for $w_n = 0$ ($\omega_p/3$ and $2\omega_p/3$) is associated with chaos (LLE = 0.04005) on the dominant frequencies regarding the third Hopf bifurcation, and exhibits the beam buckling phenomena observed even for the transverse load action. The beam subjected to the white noise ($w_n = 0.01$; 1.0) is in a chaotic regime after five Hopf bifurcations. Dynamics of the point 6 (Fig. 10) is similar to that of the point 2. Point 7 (Fig. 11) is characterized by additional fluctuations, exhibiting two-frequency quasi-periodic vibrations (ω_1 and ω_2), two Hopf bifurcations, and the intermittency phenomena. In the latter case, surprisingly the action of the noise excitation does not bring anything qualitatively new to the chaotic vibrations of the beam. Namely, when taking into account white noise of $w_n = 0.01$ and $w_n = 1$, it appeared that the beam chaotic vibrations are robust and the frequency spectra do not exhibit noisy effects.

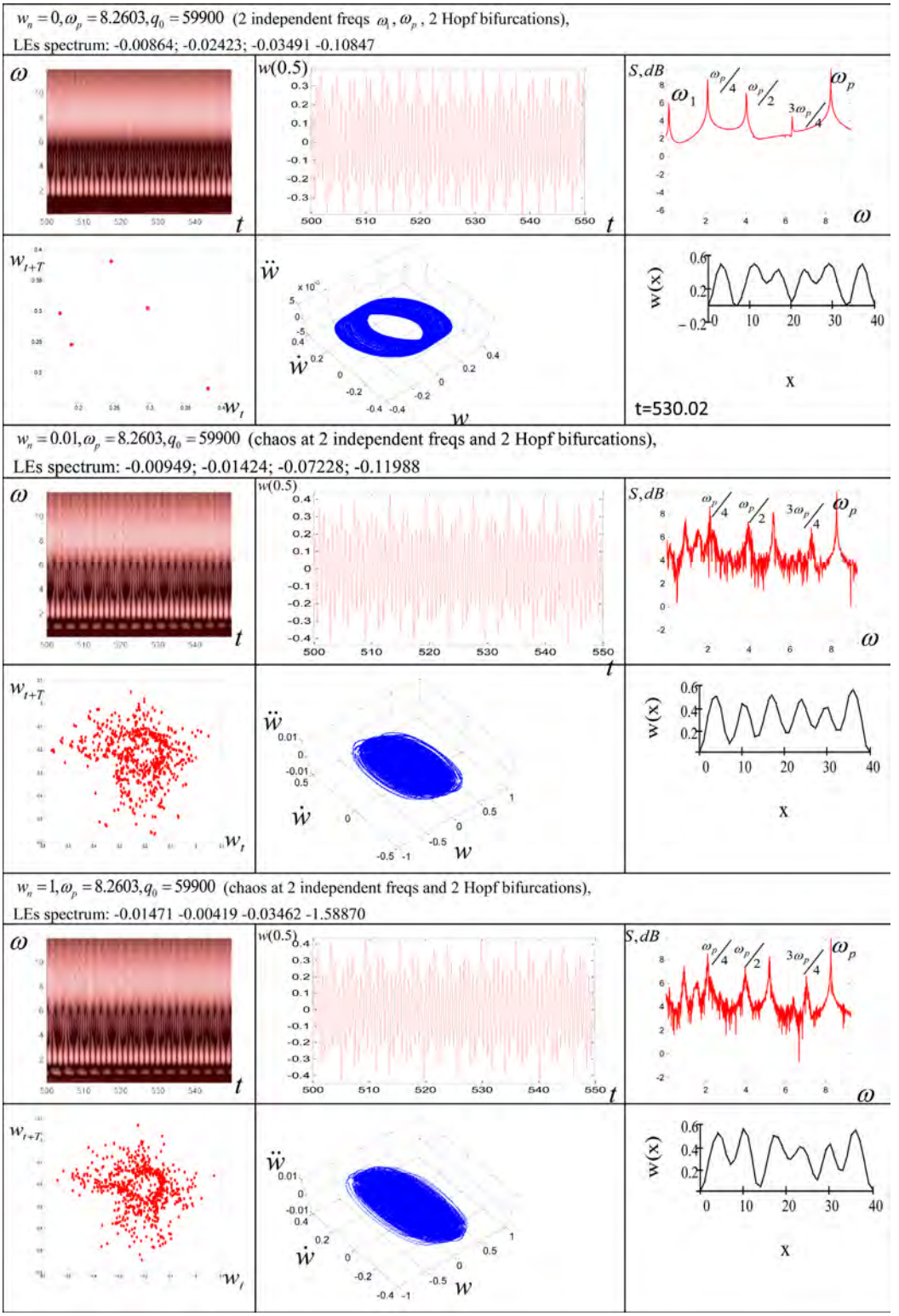

Fig. 5. The beam dynamical characteristics (2D Morlet wavelets, time histories $w(0.5;t)$, FFT, Poincaré map, 3D phase plot, beam deflection $w(x)$) for point 1.

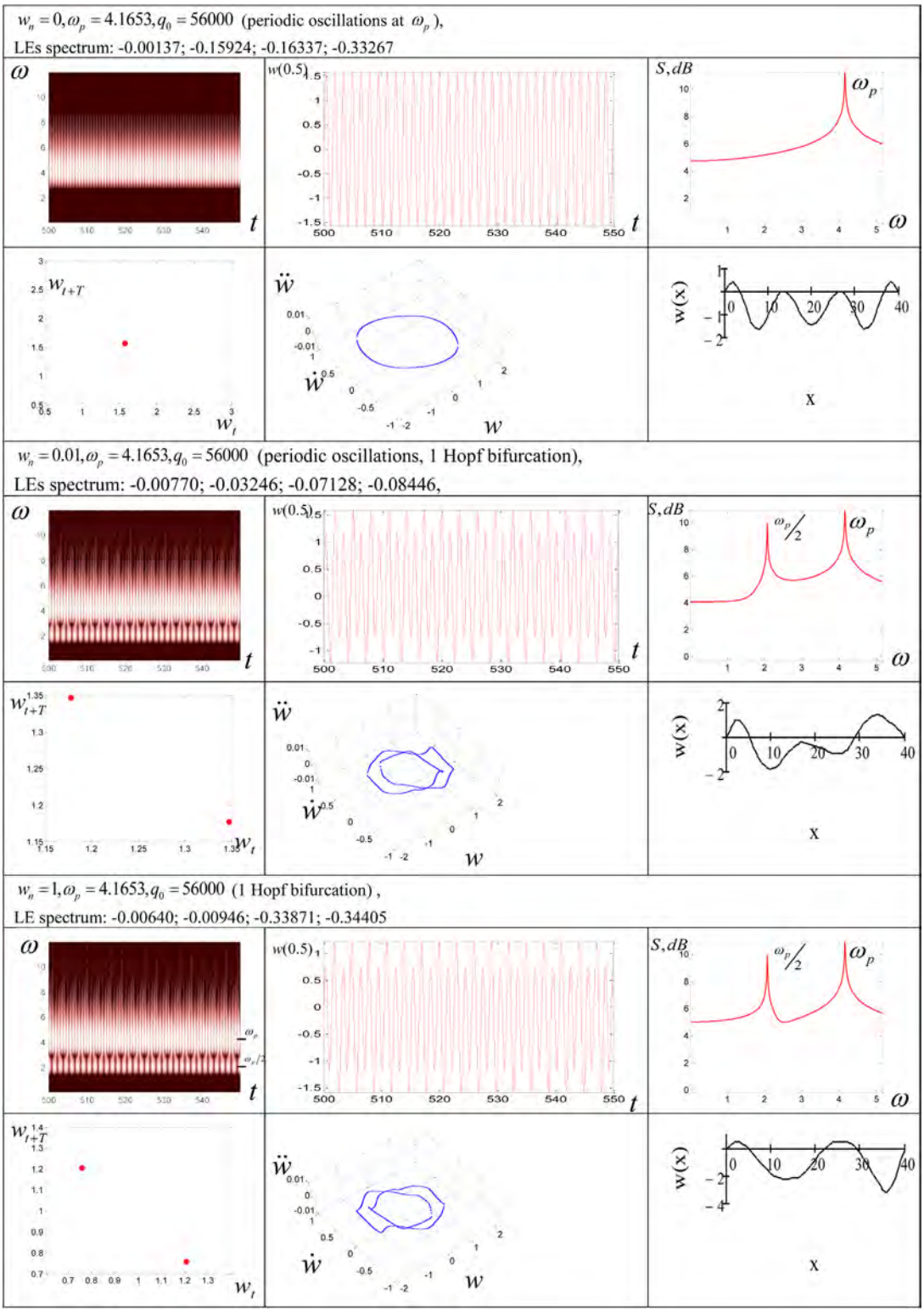

Fig. 6. Same as in Fig. 5 (point 2).

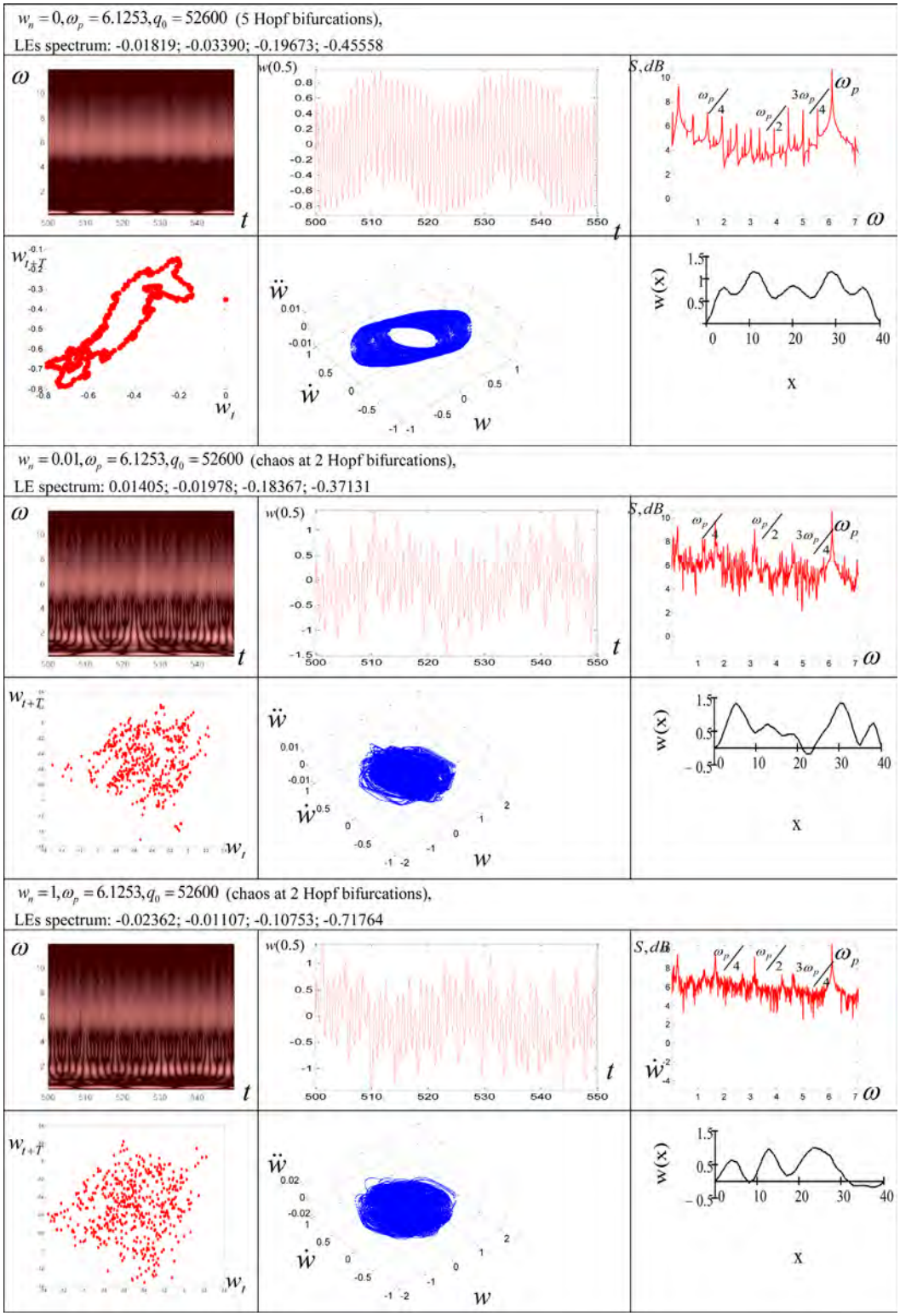

Fig. 7. Same as in Fig. 5 (point 3).

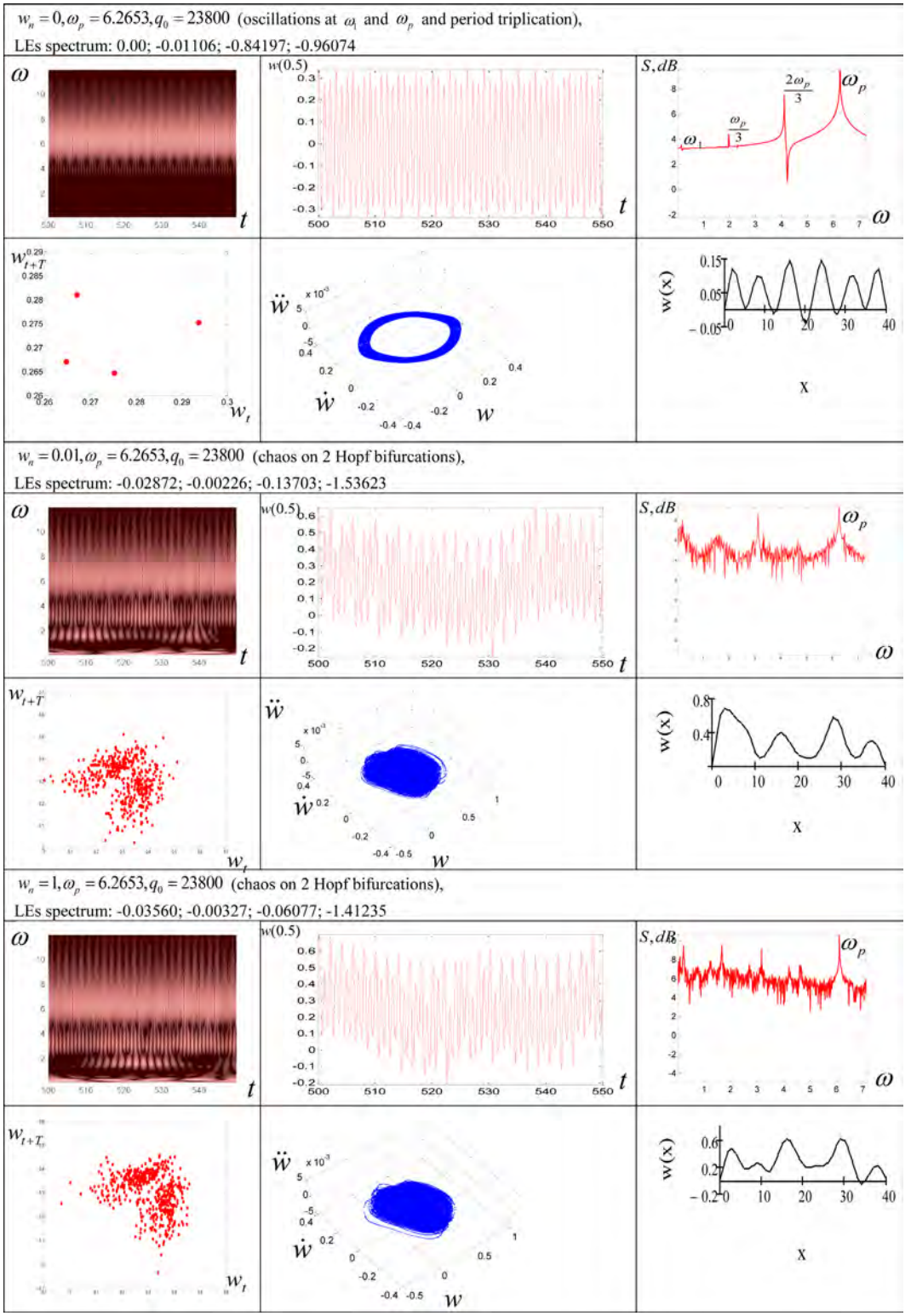

Fig. 8. Same as in Fig. 5 (point 4).

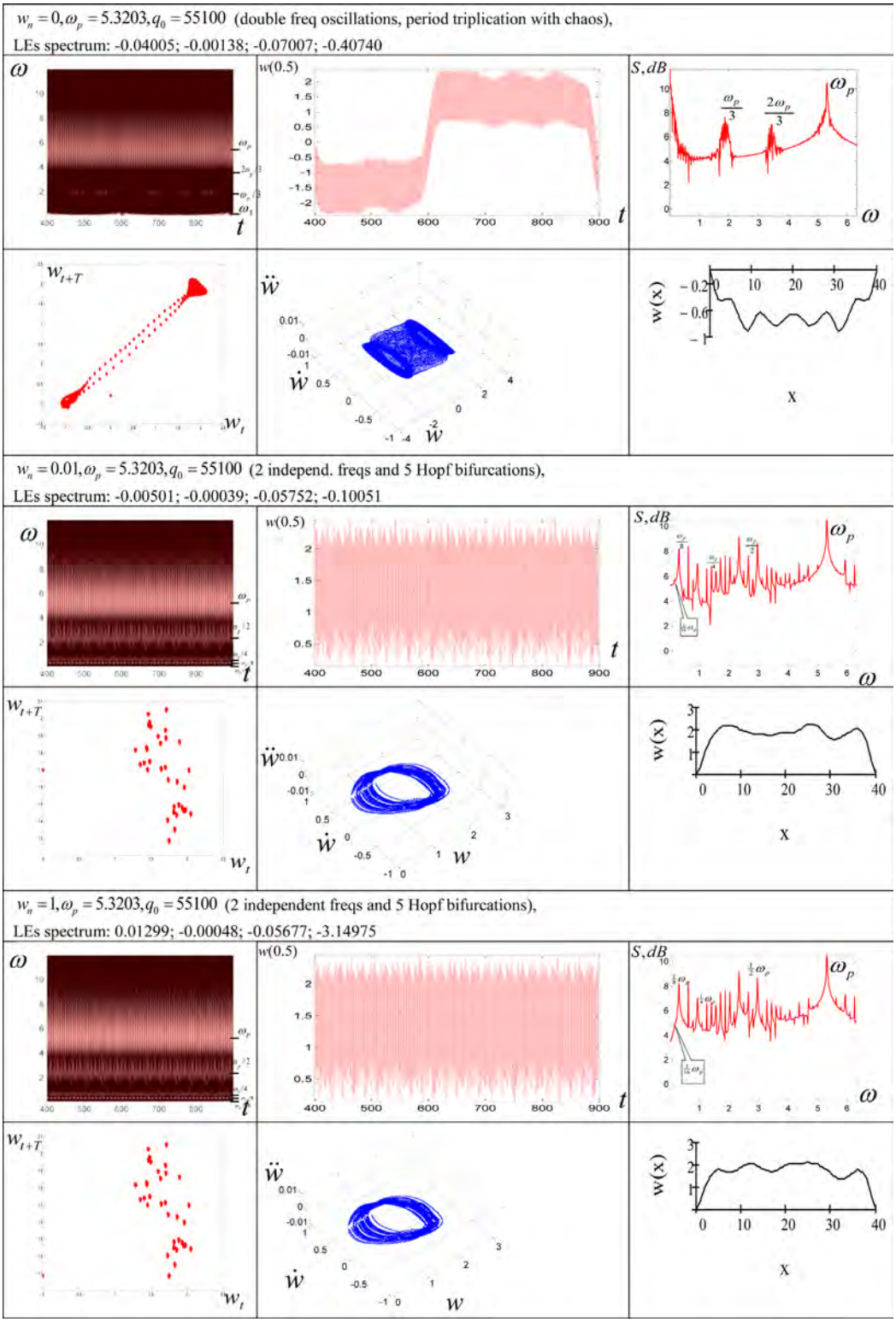

Fig. 9. Same as in Fig. 5 (point 5).

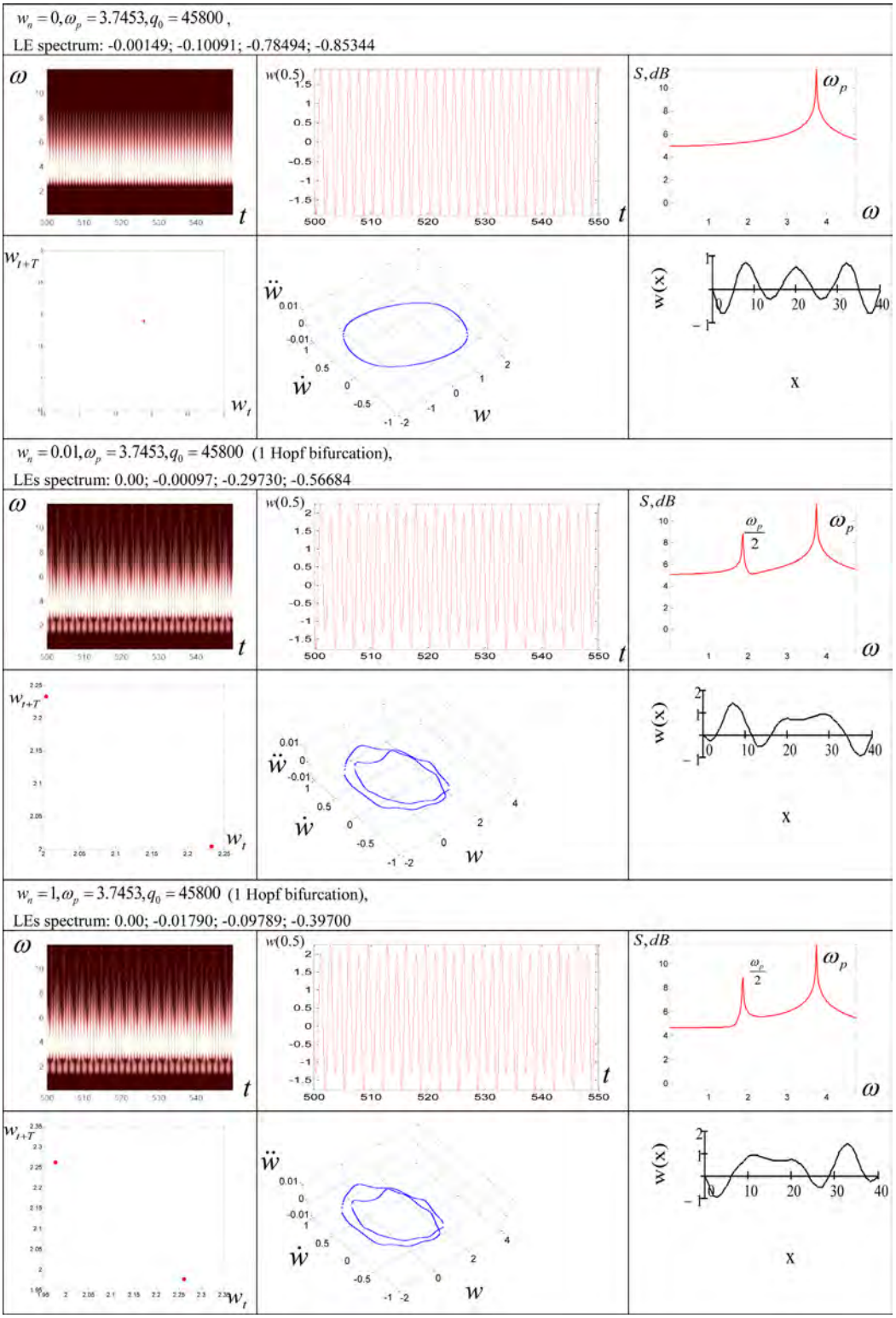

Fig. 10. Same as in Fig. 5 (point 6).

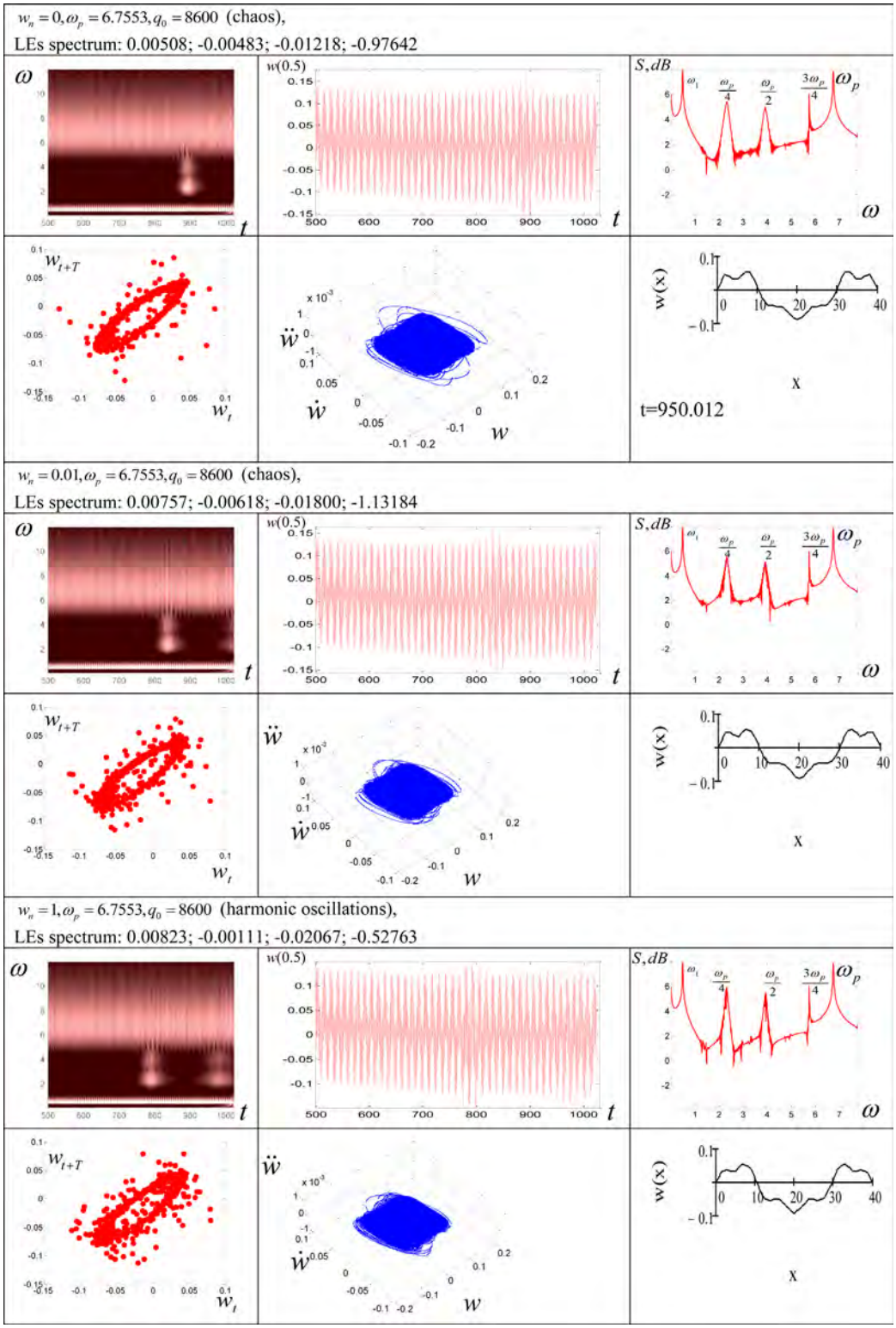

Fig. 11. Same as in Fig. 5 (point 7).

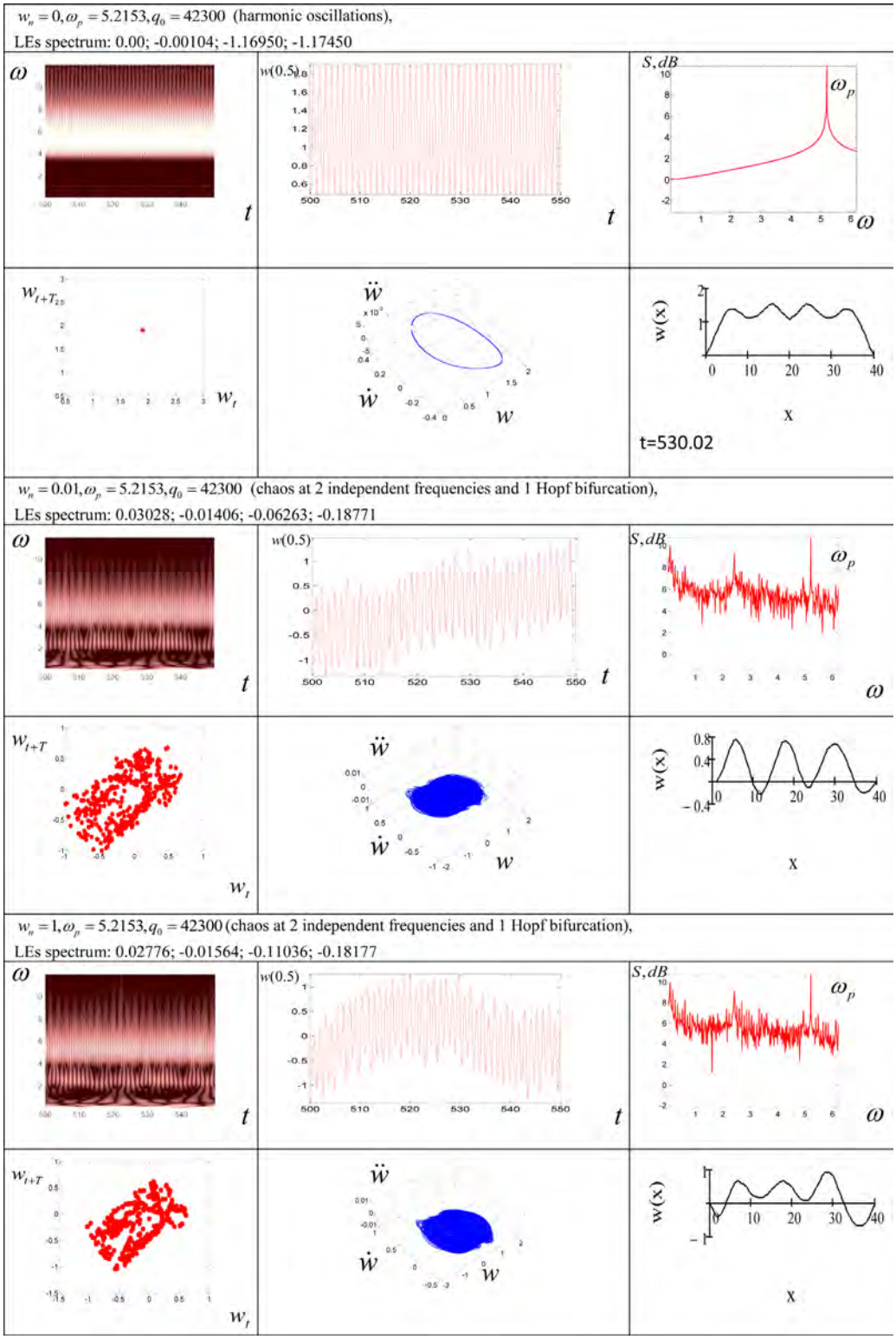

Fig. 12. Same as in Fig. 5 (point 8).

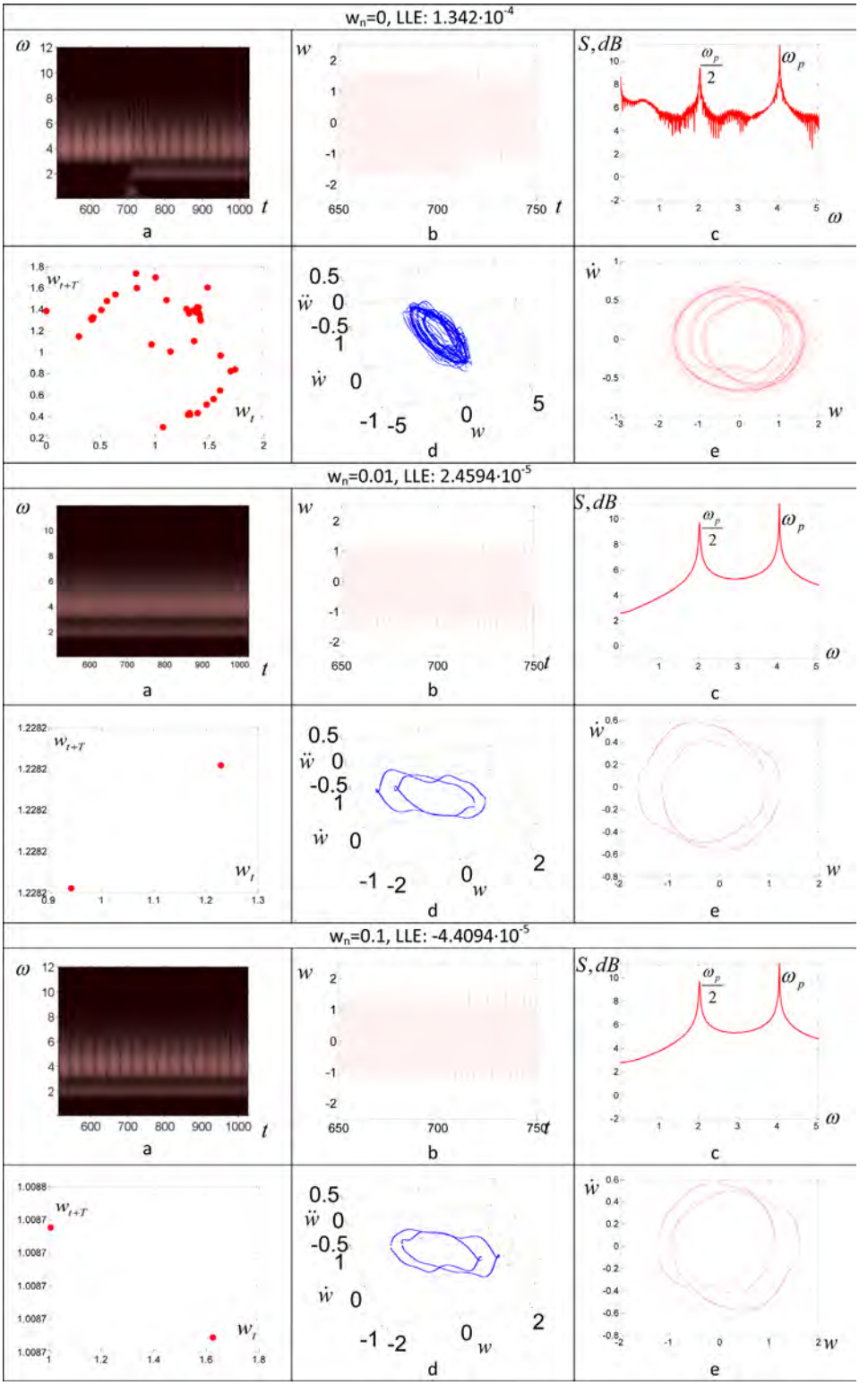

Fig. 13. The 2D Morlet wavelet spectrum, time history of the beam center, power spectrum based on FFT, Poincaré map, and 2D and 3D phase plots ($\omega_p = 4.0603, \quad q_0 = 53600$).

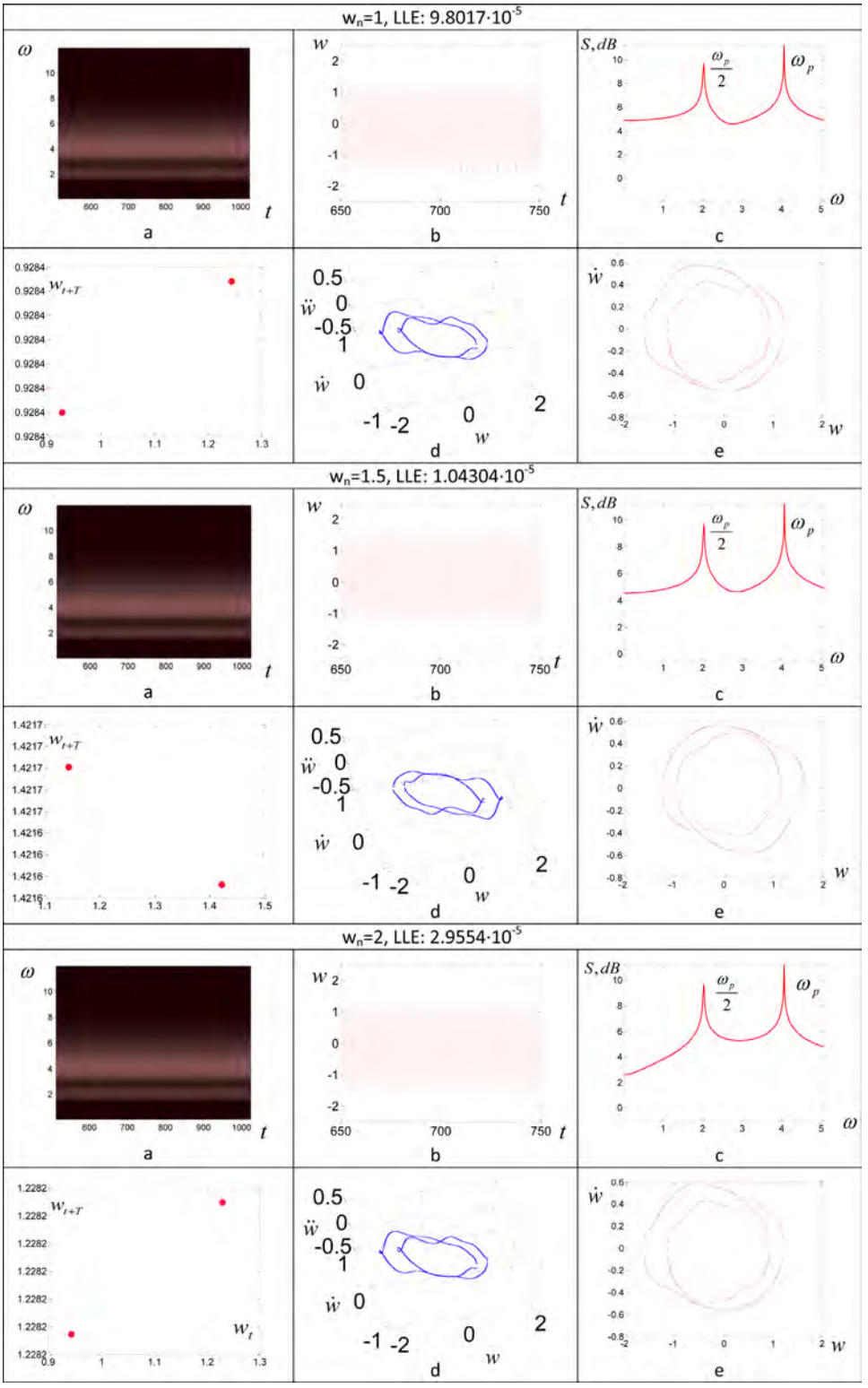

Fig. 13. (*continued*)

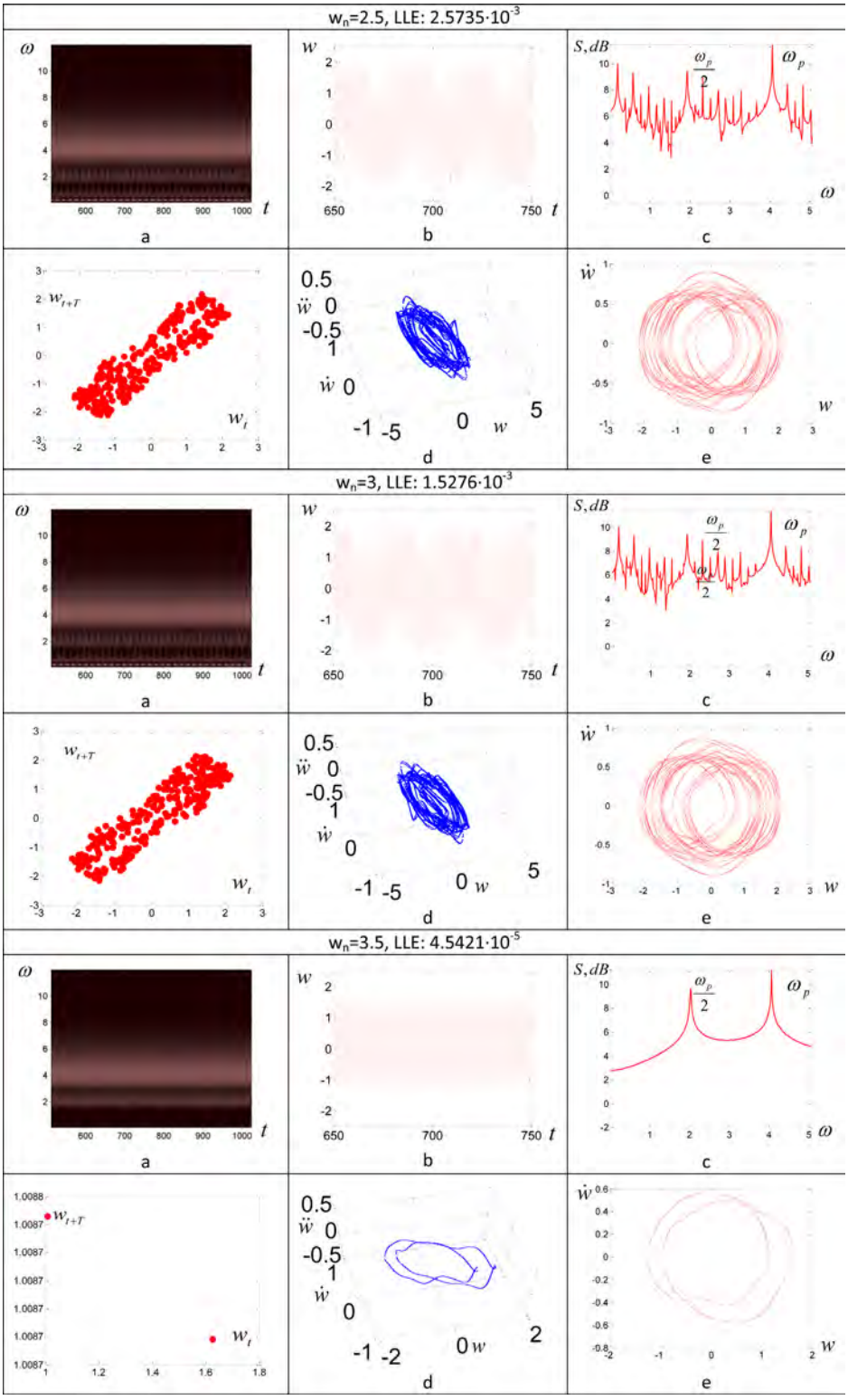

Fig. 13. (*continued*)

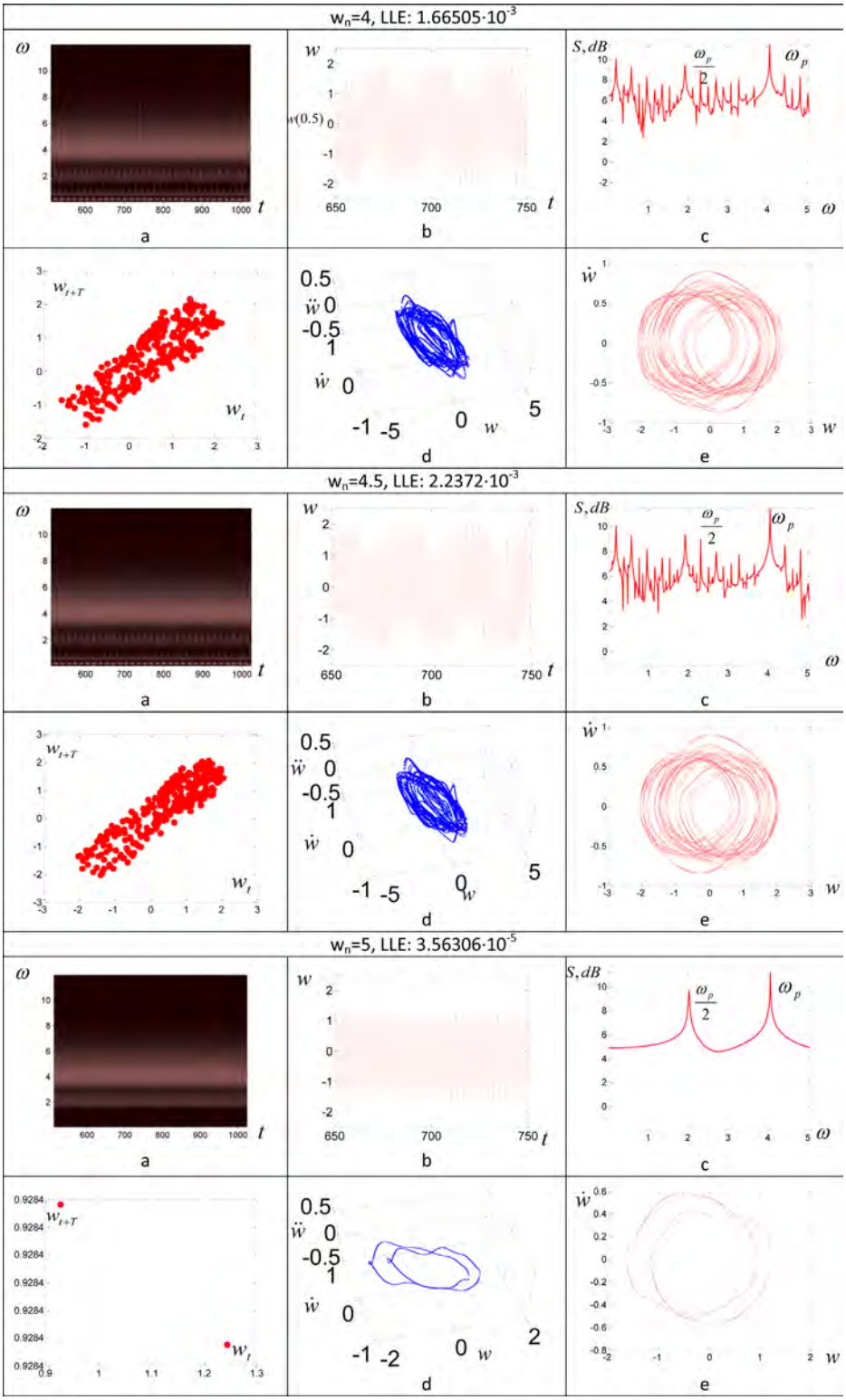

Fig. 13. (*continued*)

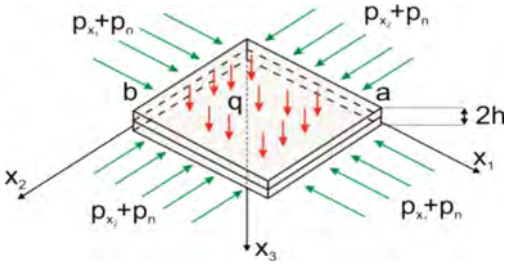

Fig. 14. The plate and its loadings.

In the point 8 (Fig. 12), a transition to chaos following the earlier described scenarios has been obtained for $w_n = 0.01$ and $w_n = 1$. Note that for $w_n = 0$ the beam exhibited periodic vibrations.

Analysis of the chart $\{q_0, \omega_p\}$ of our deterministic system (lack of white noise) shows that for low values of the frequency of the driving load, the beam vibrates periodically (Fig. 2). Increasing q_0, at low excitation frequency ω_p yields occurrence of the period-doubling bifurcations with minor zones of chaos. A change of parameter ω_p yields reduction of the bifurcation zones, and small inclusions of quasi-periodicity and chaotic zones are observed within the periodic zones. Number of partitions n has an important influence on the obtained results: zones of chaos are reduced, and zones of period-doubling bifurcations increase and merge with each other. Adding the white noise into the transverse load (Figs. 3 and 4) yields increase of both quasi-periodic and chaotic zones. In addition, at some points the transitions from periodicity to chaos and vice-versa are observed (Fig. 4). Robust dynamical states are observed at large intervals of changes regarding amplitude of the external periodic load for certain fixed frequencies. Chaotic band located at low frequencies is shown in Fig. 2.

In Figs. 5–12 graphs of the 2D Morlet wavelets, time histories of the beam center, the beam power spectra (FFT), Poincare maps, 3D phase plots and beam deflections are reported for different white noise input and different parameters of the harmonic input (ω_p, q_0). Four Lyapunov exponents are computed. As can be seen from the plots in Fig. 10 (point 6), the beam in the absence of white noise ($w_n = 0$) vibrates periodically. Even if the noise has been added ($w_n = 0.01;\ w_n = 1$) both wavelets revealed additional frequency (apparently half of the fundamental frequency). However, the noisy effects have been not visible. In the chaotic regime (point 5) alternation of vibration amplitudes of around -1.5 and $+1.5$ is seen for $w_n = 0$ (Fig. 9). The beam vibrates in a quasi-period manner for a relatively long time either around of $+1.5$ or in an unpredictable manner and then migrates to vibrate around other equilibrium state. Duration of switching between stable vibrations practically coincides with the period regarding the frequency of each vibration mode. Owing to this observation, control of the state of geometrically nonlinear beams can be realized by adding the random component of the load in the form of white noise. However, the most impressive and surprising results are shown in Fig. 13 (here only the largest Lyapunov exponent (LLE) is reported).

For $w_n = 0$ (lack of white noise) the beam vibrates chaotically and chaos is spanned on ω_p and $\omega_p/2$. In the vicinity of $t = 700$ the turbulent burst occurs (see the 2D Morlet wavelet), and the power spectrum validates occurrence of chaos after first Hopf bifurcation. It is tempting to expect that increase of noise $w_n = 0.01;2$ should increase intensity of chaotic dynamics. In contrary, already for $w_n = 0.01$ a subharmonic solution appears being validated by all used characteristics. This periodic orbit is robust against increase of the noise intensity (see the reported characteristics for $w_n = 0.01;0.1;1;1.5;2.0$). Further increase of the white noise intensity $w_n = 2.5;3$ yields a series of Hopf bifurcations, and the system transits into a chaotic regime. For $w_n = 3.5$ the chaotic attractor collapsed, and again a subharmonic vibrations appeared with the reversed symmetry with regard to the case of $w_n = 0.01$. Further increase of the noise intensity $w_n = 4;4.5$ causes occurrence of chaotic vibration, but then (for $w_n = 5$) again the subharmonic regime is exhibited.

The illustrated and discussed results imply that the noisy internal system dynamics (chaos) can be canceled by an action of the external white noise, and the systems may vibrate periodically. This shows again a possibility to control vibrations in mechanical system with infinite numbers of degrees of freedom.

5. Flexible plates

5.1. Mathematical model

We consider non-linear vibrations of flexible rectangular plate with constant stiffness and density driven both harmonically and by white noise applied along its perimeter (Fig. 14).

Plate material is assumed to be isotropic and homogeneous. The mathematical model is based on the plate Kirchhoff–Love hypotheses, whereas the geometric nonlinearity is taken into account in the form of von Kármán [37]. In the rectangular coordinate system the 3D space occupied by plate has the form: $\Omega = \{x_1, x_2, x_3 | (x_1, x_2) \in [0; a] \times [0; b], x_3 \in [-h; h]\}$,

Table 1
Estimation of the Feigenbaum constant

	1 bifurcation	2 bifurcation	3 bifurcation	4 bifurcation	5 bifurcation	Difference [%]
$p_{0,n}$	1.7	1.82	1.8473	1.853229	1.8545	
d_n		4.395604	4.604486	4.657501964		0,25

$0 \le t < \infty$. Plate vibrations are described by a system of nonlinear non-dimensional PDEs of the form [38]:

$$\begin{aligned} &\frac{1}{12(1-\mu^2)}\left(\nabla_\lambda^4 w\right) - L(w,F) - \frac{\partial^2 w}{\partial t^2} - \varepsilon\frac{\partial w}{\partial t} - q(x_1,x_2,t) = 0, \\ &\nabla_\lambda{}^4 F + \frac{1}{2}L(w,w) = 0. \end{aligned} \tag{7}$$

Here $L(w,F)$, $L(w,w)$ are known nonlinear operators, $\nabla_{\lambda_1}^4 = \frac{1}{\lambda_1^2}\frac{\partial^4}{\partial x_1{}^4} + \lambda_1^2\frac{\partial^4}{\partial x_2{}^4} + 2\frac{\partial^4}{\partial x_1{}^2 \partial x_2{}^2}$, whereas w and F are functions of deflection and stress, respectively. The system (7) is converted to dimensionless form using the following dimensionless parameters: $\lambda_1 = a/b$; $x_1 = a\bar{x}_1$, $x_2 = b\bar{x}_2$; $w = 2h\bar{w}$; $F = E(2h)^3\bar{F}$; $t = t_0\bar{t}$ – time; $q = \frac{E(2h)^4}{a^2b^2}\bar{q}$ – external normal pressure; $\varepsilon = (2h)\bar{\varepsilon}$ – environment damping coefficient. Bars over dimensionless parameters in Eq. (7) are omitted for simplicity; a, b are dimensions of the plate in plain for x_1 and for x_2, respectively; μ is Poisson's ratio. Eq. (7) should be supplemented by the boundary and initial conditions.

The system of PDEs (7) with the boundary and initial conditions is reduced by the FDM (finite difference method) to a nonlinear system of ordinary differential equations (ODEs) with the approximation $O(\Delta^2)$ of the spatial variables. The first equation of the nonlinear ODEs is solved by the Runge–Kutta fourth order method with respect to the deflection function. Further, the values of deflection are substituted into the right side of the second equation of the system (7). The second equation of (7) becomes linear and can be solved by the inverse matrix for the function force at each computational time step. The number of partitions while applying the method of finite differences is defined as $n = 14$.

5.2. The modified Feigenbaum scenario

In deterministic systems there are several scenarios of transition to chaotic oscillations that is, simple deterministic systems are able to generate internal noise (numerous results are provided in the monograph [3]). The random nature of environment is capable of inducing a much richer variety of vibration modes. It is expected to extend the classical methods of analysis to the phenomena, in which the noise plays an important role.

In what follows we include the external noise and detect and validate the transition scenarios from regular to chaotic vibrations of the rectangular plate under the longitudinal harmonic excitation load acting on the plate perimeter. We take $p_{x_1} = p_{x_2} = p_0 sin(\omega_p t)$, where ω_p, p_0 are the frequency and amplitude of the external force, respectively, and the studied time interval includes $t \in [0, 286]$ ($\lambda_1 = 1$, $\varepsilon = 1$, $\mu = 0.3$). The inhomogeneous boundary conditions are as follow:

$$\begin{aligned} &w = 0; \quad \frac{\partial^2 w}{\partial x_1{}^2} = 0; \quad F = 0; \quad \frac{\partial^2 F}{\partial x_1{}^2} = p_{x_2} + p_n \quad \text{for} \quad x_1 = 0; 1; \\ &w = 0; \quad \frac{\partial^2 w}{\partial x_2{}^2} = 0; \quad F = 0; \quad \frac{\partial^2 F}{\partial x_2{}^2} = p_{x_1} + p_n \quad \text{for} \quad x_2 = 0; 1. \end{aligned} \tag{8}$$

and the applied initial conditions follow

$$w(x_1, x_2)|_{t=0} = 0, \quad \frac{\partial w}{\partial t} = 0. \tag{9}$$

Table 2
Feigenbaum scenario obtained by wavelet transforms

$p_0 = 1.834$	$p_0 = 1.8556$	$p_0 = 1.8597$	$p_0 = 1.87$
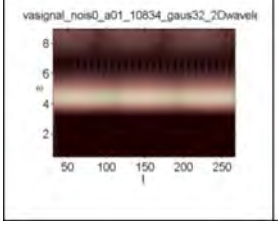	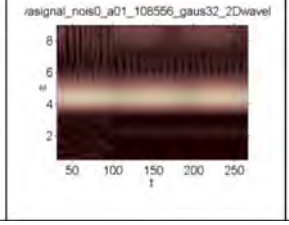	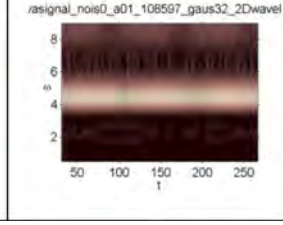	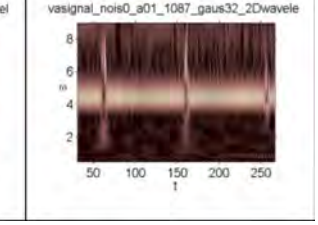

Table 3
Scenario without external fluctuations

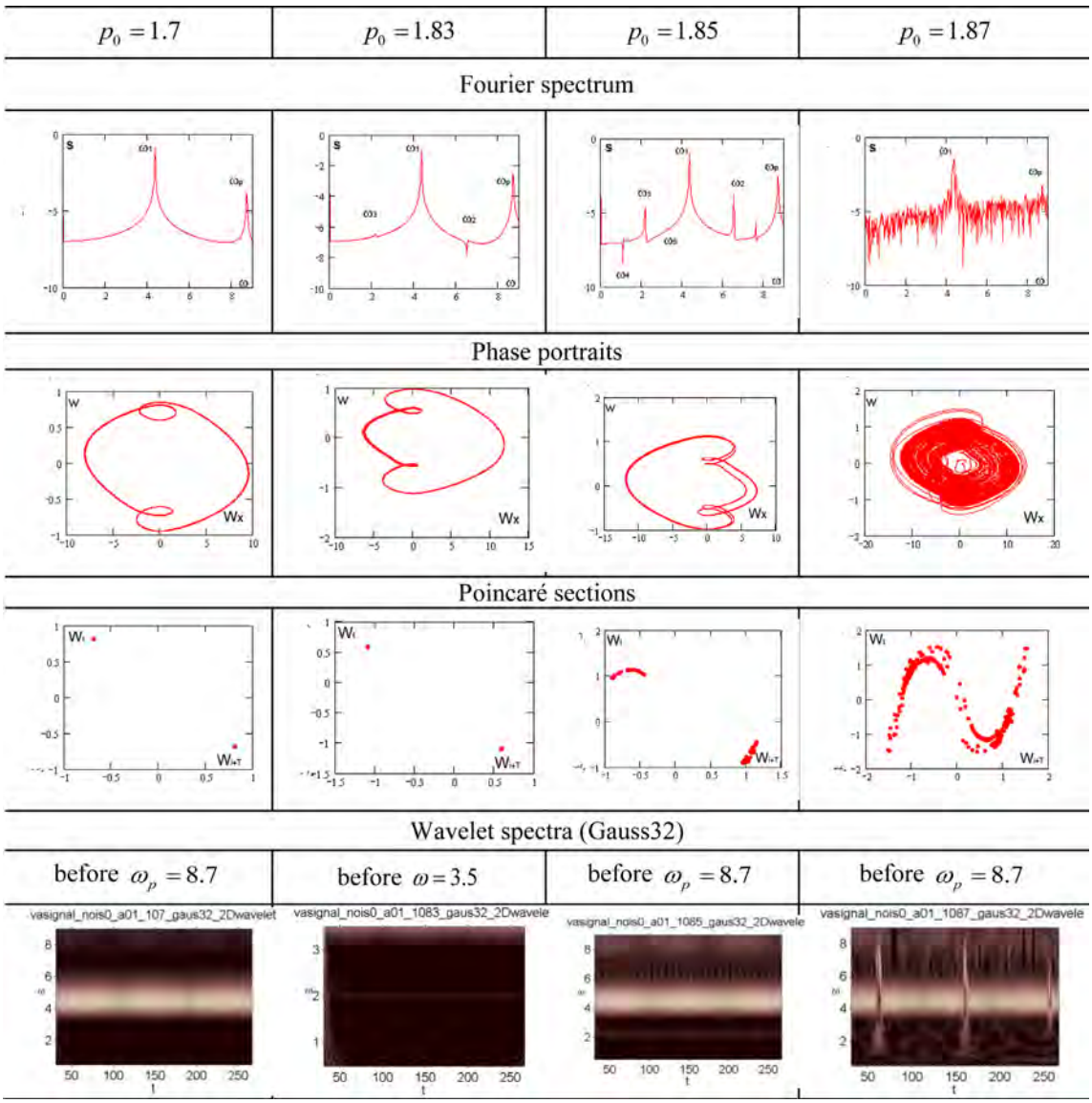

Additive noise has been added to the system in the form of random input with constant intensity $p_n = p_{n0}(2.0 \cdot rand()/(RAND\_MAX + 1.0) - 1.0)$, where p_{n0} is the intensity of the noise. It should be noted that the study of time histories obtained for the center point of the middle plate plane can be generalized to the vibrations of the remaining plate points.

Taking a frequency of the external longitudinal load $\omega_p = 8.7 > \omega_0$ (ω_0 stands for a natural frequency of the parametrically excited plate), the modified Feigenbaum scenario has been detected. The influence of the considered load (small amplitudes) yields subharmonic vibrations of the plate exhibiting a frequency equal to half of the external force frequency. Increase of the amplitude of harmonic excitation yields subharmonic plate vibrations with two frequencies, ω_p and $\omega_1 = \omega_{p/2}$. Further growth of the control parameter p_0 turns the system into a state of chaos following the modified classical scenario, i.e. containing the main features of the two classic scenarios reported by Feigenbaum and Pomeau-Manneville. As the amplitude of the external longitudinal load increases, increase of the number of Hopf bifurcations has been observed. Five consecutive doubling period bifurcations has been detected, then the time history monitored in the plate center exhibits chaotic windows with the Pomeau-Manneville intermittencies. The numerically estimated Feigenbaum constant ($d_6 = 4,663004$, Table 1) differs from the theoretical value ($d_n = 4.66916224$) by 0.25% ([4,44–45]).

Table 4
Noisy transition scenario to chaos (noise intensity $p_{n0} = 0.5$)

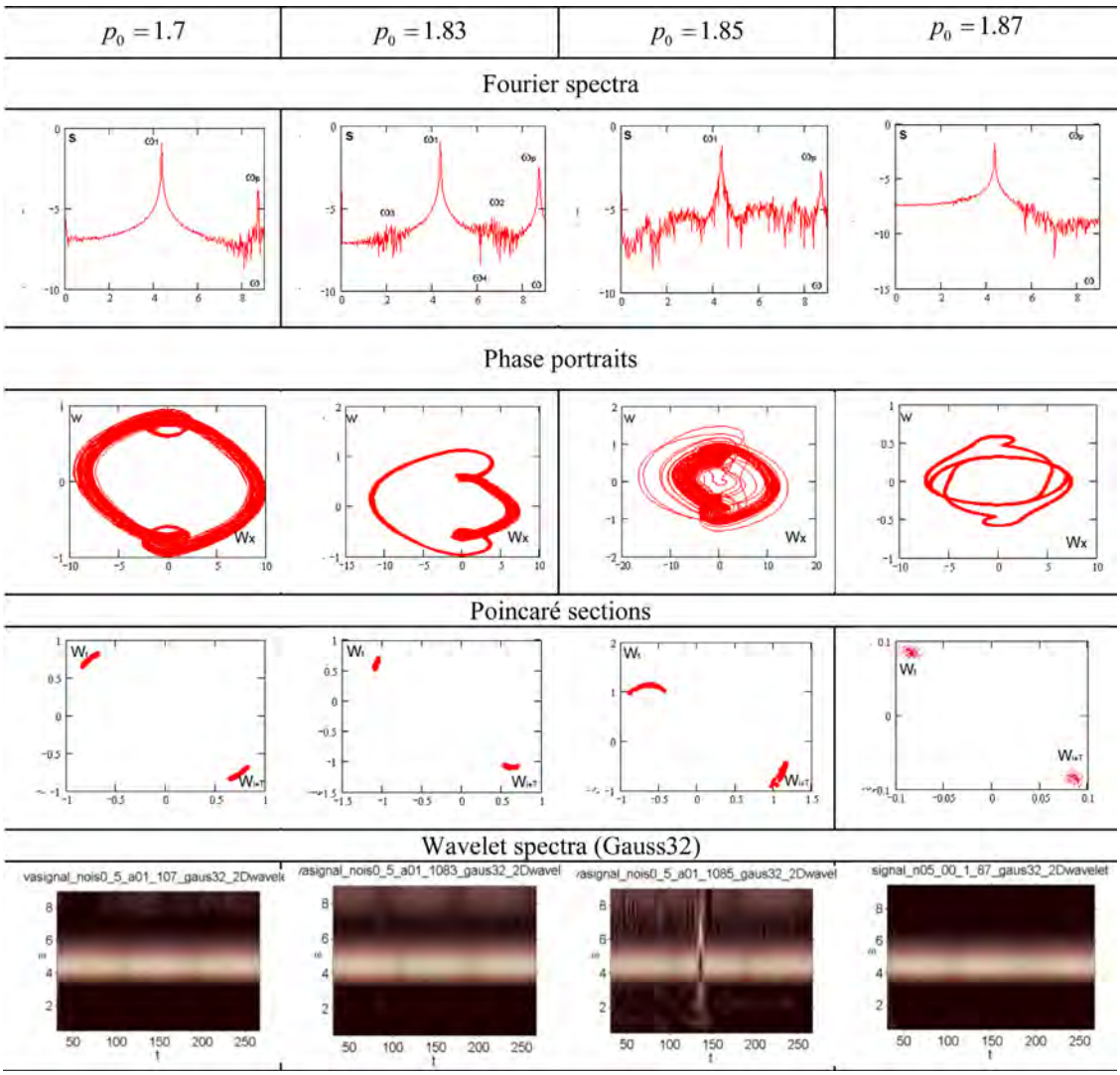

$$q(r,t) = q_0 \sin(\omega_p t) + w_n$$

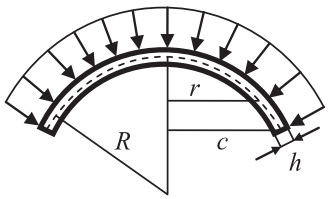

Fig. 15. Shell's scheme.

5.3. Fourier versus wavelet analysis

Wavelet theory is a powerful one being alternative to Fourier analysis, and it gives a deeper insight to the signal monitoring. The main advantage of the wavelet-analysis relies on the ability to keep track of localized features of a signal. It is well known that the Fourier coefficients represent the signal characteristics on the entire time interval. If Fourier analysis is used to analyze the signal whose characteristics change significantly over time, in the output a sum of all system behavior

Table 5
The Feigenbaim scenario and the Feigenbaum constant.

n	1	2	3	4	5	6
$q_{0,n}$	0.08	0.1335	0.13522	0.13563	0.135718	0.1357369
α_n		13.663	4.19512	4.659091	4.656084	

Table 6
EET, 2D wavelet transform and 3D phase plot of the shell center dynamics ($q_0 = 0.08$).

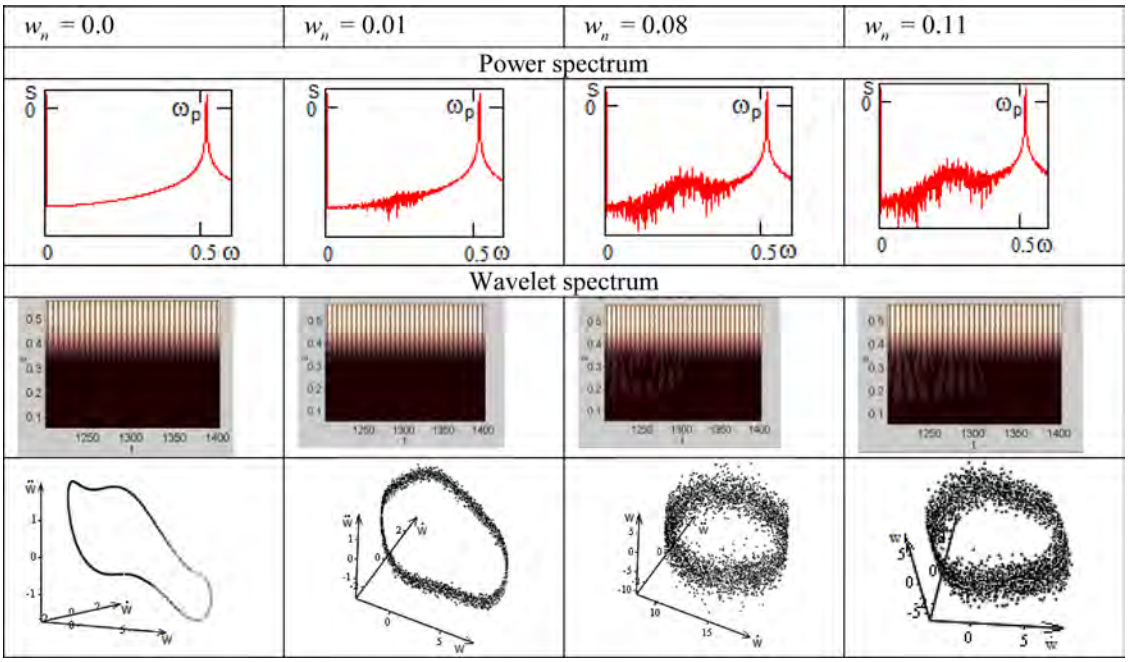

is obtained. In contrary, wavelet spectra may reveal the important features of the resulting scenario (Table 2), which cannot be detected by the standard Fourier method. First, the power of the frequencies can change in time. For instance, low frequency corresponding to the second bifurcation of period doubling, becomes visible on the wavelet spectrum at $p_0 = 1.834$ (Table 2) only for time interval $t \in (70.286)$. Advantages of the wavelets used to study chaotic dynamics of structural members are widely described in references [12,39–41,43,46].

Second, the frequency corresponding to the fourth ($p_0 = 1.853229$) and fifth ($p_0 = 1.8556$) bifurcations (see Table 2) occurs only at the initial time interval. It is important to note that these frequencies with increasing amplitude of the external longitudinal load never fill the entire spectrum. Their power seriously change over time for a fixed load. There are clearly visible zones of their "on- off" phenomena on the spectra. Also, if at a given time the frequencies of the wavelet spectrum are 'on' and corresponding to the third bifurcation, then the frequencies corresponding to the second bifurcation at this time are 'off' (see Table 2 for $p_0 = 1.8597$). Wavelet analysis of the spectra suggests that the transition to chaos is carried out via intermittency. After the fifth Hopf bifurcation, there are three chaotic windows exhibited by the wavelet spectrum. Increasing number of control parameter pushes the system to follow the Pomeau-Manneville scenario.

5.4. Additive noise actions

In this section we study the effect of additive noise intensity on the plate transition from regular to chaotic dynamics (Table 4). In Table 3 scenarios to chaos without noise action are presented. The presence of random fluctuations of the classical Feigenbaum scenario has been detected. It has been observed that increasing intensity of the external noise do not change Poincaré sections and phase portraits quantitatively. In both cases, i.e. in absence and in presence of the external noise an increase of the excitation amplitude yields chaos already after the first bifurcation. The presence of random fluctuations yields noisy Fourier power spectrum in locations corresponding to the successive bifurcations and, as a

Table 7
Same as in Table 6 ($q_0 = 0.11$).

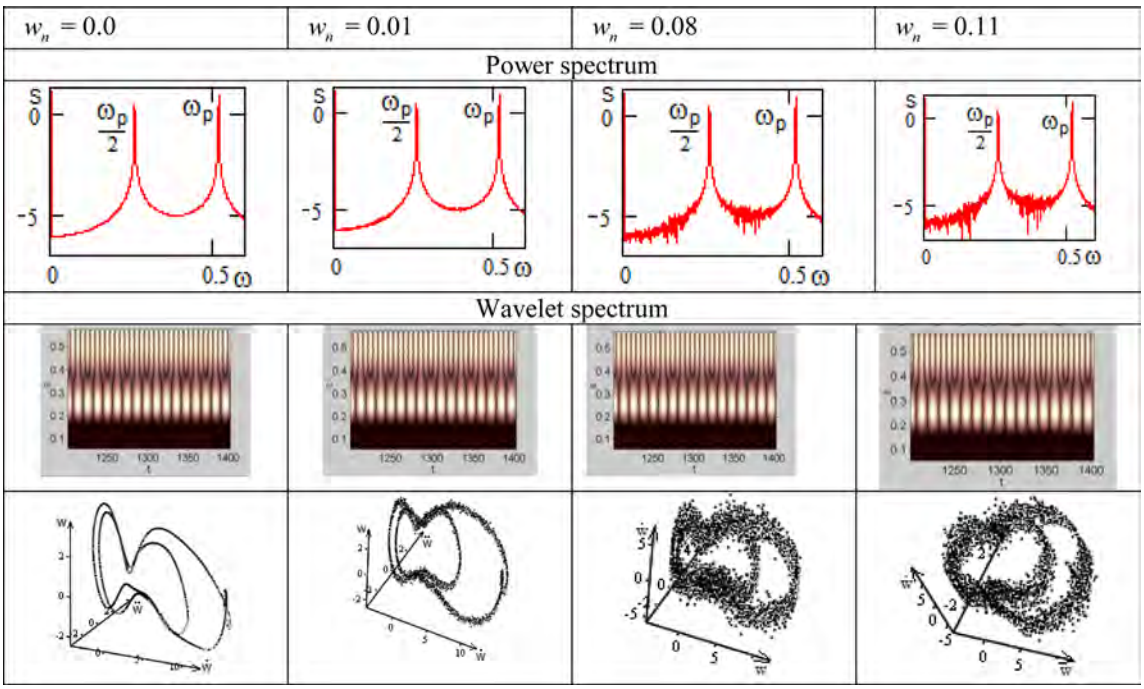

Table 8
Same as in Table 6 ($q_0 = 0.1335$).

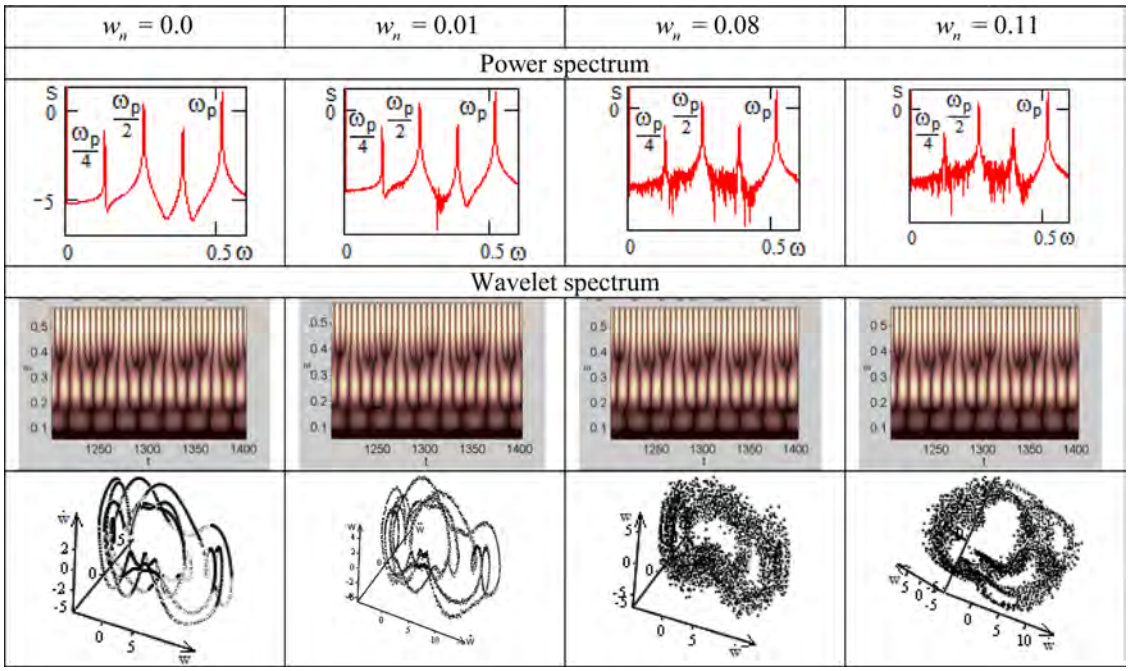

Table 9
Same as in Table 6 ($q_0 = 0.13522$).

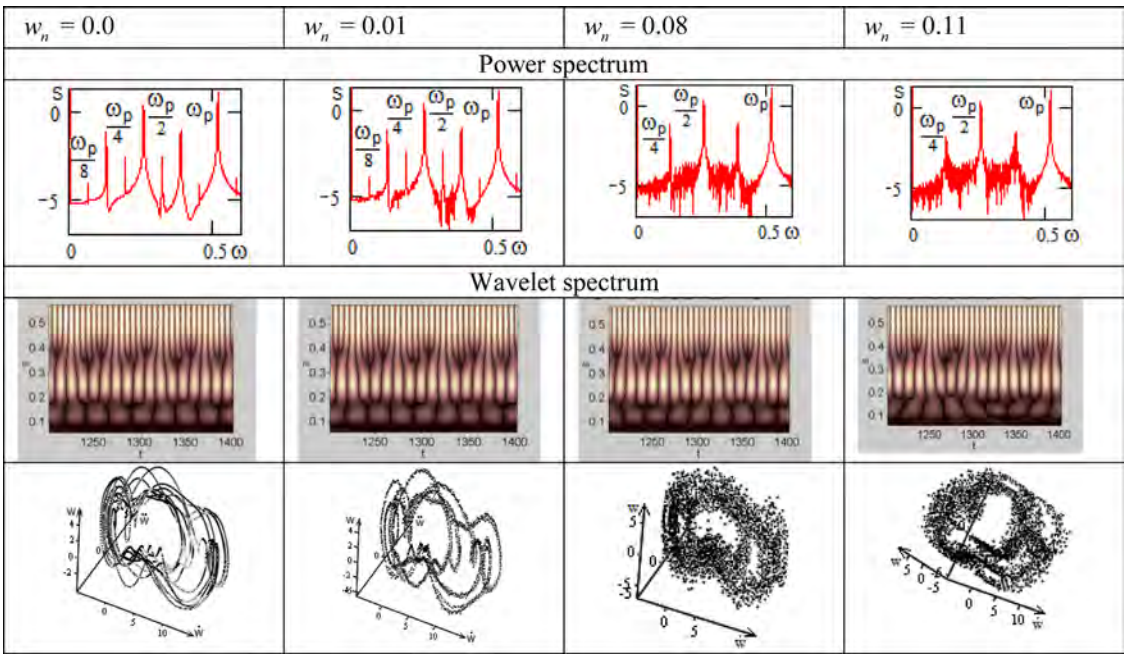

consequence, to a thickening of the phase portraits. Increase of the additive external noise intensity causes the acceleration of the emergence of the bifurcation in the plate, and consequently accelerates the transition of the system into a state of chaos.

The Gauss wavelet of the 32nd-order spectra shows that the transition to chaos of the plate external noise is carried out through intermittency. *Wavelet transforms illustrate that the state of the system changes not only by increasing control parameter (amplitude of the parametric longitudinal load), but also when its value is fixed over time.*

The frequencies corresponding to the successive bifurcations are not evenly distributed along the time axis. In contrary, the power of frequencies varies over time, and windows with "on-off" frequencies are exhibited. The wavelet spectrum constructed for the amplitude $p_0 = 1.83$ of the longitudinal load in the absence of noise shows that the frequencies corresponding to the second bifurcation of the system ($\omega_2, \omega_3 = \omega_p/4$) appear only on a small initial time interval $t \in (40, 70)$ (Table 3). However, in Table 3 the wavelet corresponding to $p_0 = 1.83$ reports the frequency range up to $\omega = 3.5$ (in order to avoid perturbations introduced by the high power frequency $\omega_p = 8.7$, and to see local features for frequency $\omega_3 = \omega_p/4$ of a much lower power). While the Fourier spectrum does not carry information about the temporal localization of these frequencies, the wavelet spectrum built for the same amplitude load ($p_0 = 1.83$) but with the intensity of the external noise $p_{n0} = 0.5$ showed that the frequencies corresponding to the second bifurcation of the system (ω_2, ω_3) appear on the whole time interval, with zone of their "on-off" effects. The frequency corresponding to the next bifurcation in this experiment ($p_{n0} = 0.5$) appears at $p_0 = 1.85$, which has been reported for the time interval $t \in (125, 150)$.

Taking into account the so far carried out analysis, one may conclude that the wavelet transform approach yields deeper investigations of the features of noise-induced transitions in the considered structural members (here plate) versus the intensity of the external additive noise. Constructed wavelets show that increasing the intensity of the noise component involves "more sparse spectrum" exhibited by the range of the low frequencies. Power of frequencies corresponding to the second and subsequent bifurcations are located significantly below the power of the frequency $\omega_1 = \omega_p/2$. The higher the intensity of white noise, the smaller zones of "inclusion" of frequencies corresponding to the seconds and subsequent bifurcations. It is worthy to mention that in the absence of external noise, as well as in it presence, if on the wavelet spectrum at the certain time moment the frequencies corresponding to the third bifurcation are "on", then the frequencies corresponding to the second bifurcation at this time instant are "off".

Increasing the amplitude of the longitudinal external load, the subharmonic plate vibrations $\omega_p/2$ appear in the experiments with higher intensity noise. However, the so far mentioned non-linear effects have not been found while monitoring of the transition into chaos in the absence of the random noise.

Table 10
Same as in Table 6 ($q_0 = 0.14$).

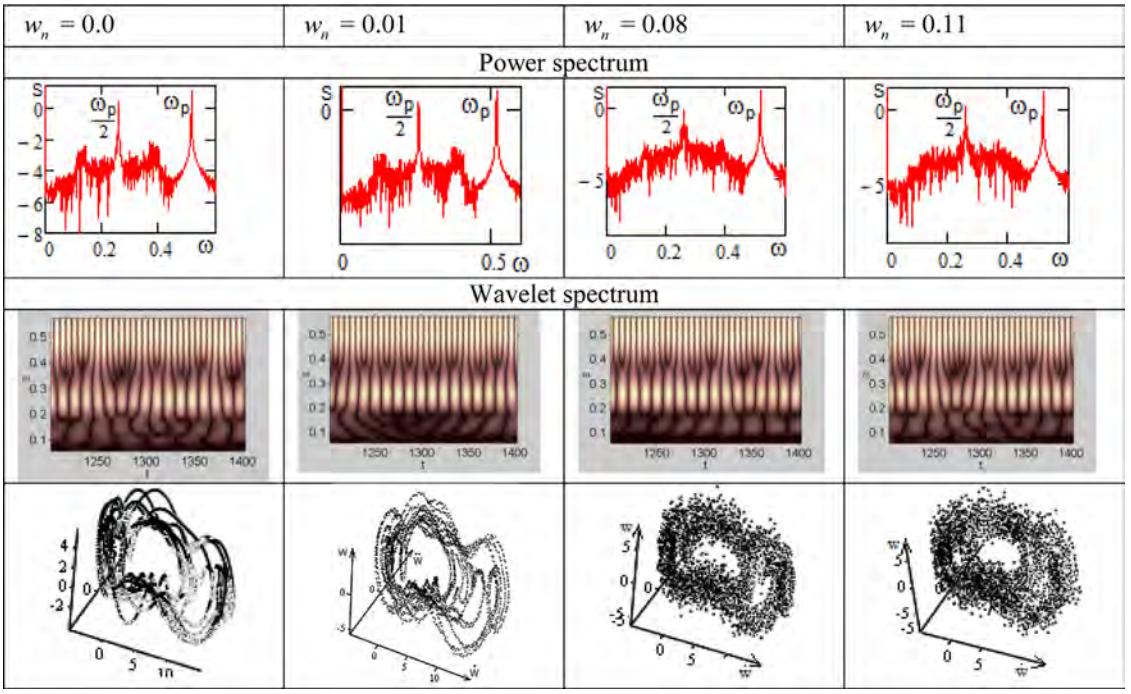

6. Shells

6.1. Mathemmatical model

We consider a spherical shallow shell in a polar coordinate system, introduced as follows: $\Omega = \{(r, z) | r \in [0, b], -h/2 \le z \le h/2\}$. The system of equations of the nonlinear axially symmetric vibrations of the shell has the following form [38] (see Fig. 15):

$$\frac{\partial^2 w}{\partial t^2} + \varepsilon \frac{\partial w}{\partial t} = -\frac{\partial^4 w}{\partial r^4} - \frac{2}{r}\frac{\partial^3 w}{\partial r^3} + \frac{1}{r^2}\frac{\partial^2 w}{\partial r^2} - \frac{1}{r^3}\frac{\partial w}{\partial r} - \frac{\Phi}{r}\left(1 - \frac{\partial^2 w}{\partial r^2}\right) - \frac{\partial \Phi}{\partial r}\left(1 - \frac{1}{r}\frac{\partial w}{\partial r}\right) + 4q(r,t),$$

$$\frac{\partial^2 \Phi}{\partial r^2} + \frac{1}{r}\frac{\partial \Phi}{\partial r} - \frac{1}{r^2}\frac{\partial \Phi}{\partial r} = \frac{\partial w}{\partial r}\left(1 - \frac{1}{2r}\frac{\partial w}{\partial r}\right), \quad \Phi = \frac{\partial F}{\partial r}. \tag{10}$$

Here we have introduced the dimensionless quantities: $\bar{t} = \omega_0 t$; $\omega_0 = \sqrt{Eg/\gamma R^2}$; $b = \left(c/\sqrt{Rh}\right)$; $\bar{\varepsilon} = \varepsilon R/h\sqrt{g/(\gamma E)}$, $\bar{F} = \eta F/Eh^3$; $\bar{w} = w\sqrt{\eta}/h$; $\bar{r} = br/c$; $\eta = 12(1-\nu^2)$; $\bar{q} = \bar{q}_3 = (R/h)^2 q_3\sqrt{\eta}/(4E)$; where t – time; ε – the viscosity of the environment, in which the shell moves; F – Airy's function; w – shell deflection; R, c – main curvature radius of the shell at the support profile and the radius of the support profile, respectively; h – shell thickness; b – flatness parameter; ν – Poisson's ratio; r – distance from the axis of rotation to the point on a median surface; $q(r, t)$ - external load excitation; ω_0 – natural frequency. Bars over dimensionless quantities in (10) are already omitted. Eq. (10) requires boundary and the initial conditions, and the conditions at the shell top follow:

$$\Phi \approx Ar, \quad \Phi' \approx A, \quad w \approx B + Cr^2, \quad w' \approx 2Cr, \quad w'' \approx 2C, \quad w''' \approx 0. \tag{11}$$

In order to transform the continuous system (10) to a system with lumped parameters, we use the method of finite differences with the order of approximation $O(\Delta^2)$(the applied load may vary according to any law). In this paper we have investigated the shell vibrations under the action of the alternating load conditions in the presence of external noise, i.e.$q(r, t) = w_n(2.0 * \text{rand}()/(\text{RAND\_MAX} + 1.0) - 1.0) + q_0 \sin(\omega_p t)$, where w_n stands for the intensity of the Gaussian white noise, q_0 is the amplitude of the driving load, ω_p is the frequency of the harmonic excitation. After reducing the problem (10) to the normal Cauchy problem, the obtained ODEs are solved by the fourth-order Runge–Kutta method. The time step is chosen from the condition of stability of the solution ($\Delta t = 3.90625 \cdot 10^{-3}$).

6.2. Classical and modified scenarios

The Feigenbaum scenario associated with transition from regular to chaotic vibrations has been detected. The Feigenbaum model [4,44–45] has been sufficiently validated by numerous numerical experiments but devoted to simple mathematical models. On the other hand, it is also known that period doubling bifurcation is exhibited by the Rőssler attractor, and many others [3]. This classical route of transition to chaos has also been found in our problem, though it has infinite dimension. Feigenbaum scenario has been detected by noisy excitation of the spherical shell with hinged-moving support profile and the excitation frequency $\omega_p = 0.516$. For hinged-moving support in the meridional direction, the boundary conditions can be written as follows:

$$\Phi = w = 0, \quad \frac{\partial^2 w}{\partial r^2} + \nu \frac{\partial w}{\partial r} = 0 \quad r = b, \tag{12}$$

and the following initial conditions are applied:

$$w = f_1(r,0), \quad w' = f_2(r,0). \tag{13}$$

Eq. (10) is supplemented by the boundary (12) and the initial conditions (13). Table 5 reports numerically estimated period doubling bifurcation scenarios and the Feigenbaum constant versus the control parameter q_0 in the absence of external noise ($b = 4$).

The Feigenbaum constant yielded by our numerical experiments

$$\alpha_n = \frac{q_{0,\,n} - q_{0,n-1}}{q_{0,n+1} - q_{0,\,n}} = 4.65608466, \quad n = 6 \tag{14}$$

is in very good agreement with the theoretical counterpart value $\alpha_6 = 4.66916224$ (difference is about 0.28%).

In what follows we describe computational results obtained for the studied flexible spherical shell with the added noisy component, depending on the increase of amplitude intensity of the external load at a fixed intensity of additive Gaussian white noise. We have analyzed signals (time histories), phase portraits, the Fourier spectra and the wavelet transforms. It should be emphasized that in order to get reliable results we need to analyze together the Fourier and wavelet spectra as well as phase portraits. Fourier spectrum gives the integral characteristics, whereas the wavelet spectrum allows to carry out more detailed analysis. Namely, to determine how the frequency change in time, to detect and observe intermittency phenomena, to determine the length of the laminar and chaotic signal fluctuations, etc., Fourier and wavelet transforms are applied. The obtained results are shown in Tables 6–10. First, we have investigated the effect of the intensity of additive white noise on the classical Feigenbaum scenario. The overall analysis of the characteristics shows that our shell with noisy excitation exhibits the Hopf bifurcation at lower load values (Table 6) than in the case without noise. The localization of frequencies takes place around the first bifurcation ($w_n = 0.01$). After the emergence of the bifurcation, localization occurs around the next bifurcation, and so on (Tables 6–10). The structure of the phase portrait changes: the greater intensity of the noise fluctuations, the more "scatters" at the domain of phase trajectories attraction. This is especially evident in the phase portraits reported in the Tables 6–10 at $w_n = 0.08$ and at $w_n = 0.11$. The increase in the intensity of a Gaussian white noise with fixed amplitude of the external excitation $q_0 = 0.08$ yields the increase of the number of frequencies in the power spectrum (in the wavelet spectrum "on" and "off" zones are observed for $w_n = 0.08$ and $w_n = 0.11$).

At a low noise level of $w_n = 0.01$, the classical Feigenbaum scenario does not change, but it is accompanied by the noisy spectrum components. After the first Hopf bifurcation with increasing amplitude of the external alternating load $q_0 = 0.11$ (Table 7) the frequencies localization appears around the second bifurcation at $w_n = 0.01$, and the wavelet spectrum shows constant frequencies over time. Further increase of the of the external load amplitude $q_0 = 0.1335$ and $q_0 = 0.13522$ (Tables 8 and 9) yields also localization of frequencies in the power spectrum around the third and fourth bifurcation values, respectively, under low-intensity white noise $w_n = 0.01$. Further increase of the external amplitude load q_0 (in the absence of noise) leads to new Hopf bifurcations. Addition of the white noise makes power spectrum "noisy" already under the load $q_0 = 0.13535$, i.e. chaos occurs rapidly. In the small noise action $w_n = 0.01$, four Hopf bifurcations have been detected, but the Feigenbaum constant is several times higher than the theoretical value. A further increase of the excitation amplitude leads to "destruction" of the period-doubling frequencies, and transition to the chaotic state via the first Hopf bifurcation. Increasing the intensity of the additive noise ($w_n = 0.08$ and $w_n = 0.11$) allows to conclude that after the second bifurcation power spectrum becomes so noisy, that the presence of the third, fourth, etc. bifurcations cannot be determined.

Phase portrait shows that the distance between the phase trajectories is influenced by low-intensity white noise. Increasing the amplitude of the noise increases the distance between the chaotic phase trajectories ($w_n = 0.08$, $w_n = 0.11$ and $q_0 = 0.14$), but the power spectra and wavelet analysis show chaotic vibrations associated with the second bifurcation. *It should be emphasized that only joint analysis of the Fourier and wavelet spectra, and spatial phase portrait, makes it possible to characterize properly the dynamical state of our mechanical system.* Further increase of the white noise intensity did not introduce anything qualitatively new to the shell vibrations character.

7. Conclusions

In our previous published papers and monographs we have reported numerous advantages of the developed general approach to study chaotic dynamics of structural members (beams, panels, plates, and shells). The given earlier and applied here theoretical background consists of two main steps: (i) Application of a proper and economical reduction procedure of the governing PDEs to ODEs preserving all non-linear features and correspondence of the introduced mathematical and physical modeling of the structural members with an emphasis on validation and reliability of the obtained results; (ii) Application of the wavelet based analysis to follow frequencies temporal behavior, which strongly improves and validates results obtained by the applied classical numerical characteristics of the dynamical non-linear phenomena. The carried out review of the state of art of the research devoted to the similar like problems shows that there is a lack of the similar approaches to study non-linear dynamical behavior of structural members. This paper can be viewed as the extension of our widely applied theoretical/numerical methods to study continuous structural members subjected to external additive white noise.

The following general observations and results are yielded by our investigations:

1. The investigated structural members have shown a few different scenarios of transition from periodic to chaotic vibrations in absence of white noise. In spite of already known and well documented scenarios, like the Feigenbaum, the Ruelle-Takens-Newhouse and the Pomeau-Manneville routes to chaos, there exist also other scenarios being modifications of the known scenarios.
2. We have detected, illustrated and discussed the modified Feigenbaum scenario, which is a combination of the classical Feigenbaum and Pomeau-Manneville scenarios.
3. The presence of small noise significantly reduces the area of regular zones existence in the parameter planes, which has been reported on the charts of vibrations kind.
4. Applied random fluctuations may either destroy or amplify the scenarios of transition from regular to chaotic dynamics structural members for the same fixed system of parameters.

Acknowledgment

This work has been supported by the Polish National Science Centre, MAESTRO 2, No. 2012/04/A/ST8/00738.

References

[1] D. Ruelle, F. Takens, On the nature of turbulence, Commun. Math. Phys. 20 (1971) 167–192.
[2] P. Manneville, Y. Pomeau, Different ways to turbulence in dissipative dynamical systems, Phys. D 1 (2) (1980) 219–226.
[3] J.C. Sprott, Elegant Chaos, World Scientific, Singapore, 2010.
[4] M. Feigenbaum, The transition to aperiodic behavior to turbulent systems, Commun. Math. Phys. 77 (1980) 65–86.
[5] J. Awrejcewicz, V.A. Krysko, Feigenbaum scenario exhibited by thin plate dynamics, Nonlinear Dyn. 24 (4) (2001) 373–398.
[6] J. Awrejcewicz, A.V. Krysko, Analysis of complex parametric vibrations of plates and shells using Bubnov-Galerkin approach, Arch. Appl. Mech. 73 (7) (2003) 495–503.
[7] J. Awrejcewicz, V.A. Krysko, A.F. Vakakis, Nonlinear Dynamics of Continuous Elastic System, Springer, Berlin, 2004.
[8] J. Awrejcewicz, V.A. Krysko, A.V. Krysko, Complex parametric vibration of flexile rectangular plates, Meccanica 39 (3) (2004) 221–224.
[9] J. Awrejcewicz, V.A. Krysko, A.V. Krysko, Thermo-Dynamics of Plates and Shells, Springer, Berlin, 2007.
[10] V.A. Krysko, I.V. Papkova, V.V. Soldatov, Analysis of nonlinear chaotic vibrations of shallow shells of revolution by using the wavelet transform, Mech. Solids 45 (1) (2010) 85–93.
[11] V.A. Krysko, I.V. Kravtsova, Control of chaotic vibrations in flexible spherical shells, Mech. Solids 41 (1) (2006) 124–134.
[12] V.A. Krysko, J. Awrejcewicz, G.G. Narkaitis, Bifurcations of twin plate – strip excited transversally and axially, Nonlinear Dyn. 32 (2) (2003) 187–209.
[13] V.A. Krysko, J. Awrejcewicz, G.G. Narkaitis, Nonlinear vibration and characteristics of flexible plate-strips with non-symmetric boundary conditions, Commun. Nonlinear Sci. Num. Simul. 11 (1) (2006) 95–124.
[14] T.S. Krasnopolskaya, A. Yu, Shvets, Dynamical chaos for a limited power supply oscillations in cylindrical tanks, J. Sound. Vib. 322 (2009) 532–553.
[15] A.Yu Shvets, V.O. Sirenko, Peculiarities of transition to chaos in nonlinear hydrodynamics systems, Chaotic Model. Simul. J. 2 (2012) 303–310.
[16] W. Zhang, F. Wang, M. Yao, Global bifurcations and chaotic dynamics in nonlinear nonplanar oscillations of a parametrically excited cantilever beam, Nonlinear Dyn. 40 (3) (2005) 251–279.
[17] P. Ribeiro, Non-linear forced vibrations of thin/thick beams and plates by the finite element and shooting methods, Comput. Struct. 82 (17–19) (2004) 1413–1423.
[18] J. Fang, I. Elishakoff, Nonlinear response of a beam under stationary random excitation by improved stochastic linearization method, Appl. Math. Model. 19 (1995) 106–111.
[19] T. Dahlberg, The effect of modal coupling in random vibration analysis, J. Sound Vib. 228 (1) (1999) 157–176.
[20] R.G. Jacquot, Random vibration of damped modified beam systems, J. Sound Vib. 234 (3) (2000) 441–454.
[21] S. Kukla, B. Skalmierski, The effect of axial loads on transverse vibrations of an Euler-Bernoulli beam, J. Theor. Appl. Mech. 2 (31) (1993) 413–430.
[22] G. Janevski, P. Kozic, R. Pavlovic, Z. Golubovic, The moment Lyapunov exponent of a Timoshenko beam under bounded noise excitation, Arch. Appl. Mech. 81 (2011) 403–417.
[23] M. Collet, E. Foltete, C. Iexcellent, Analysis of the behavior of a shape memory alloy beam under dynamical loading, Eur. J. Mech. 20 (2001) 615–630.
[24] M.A. Savi, P.M. Pacheeo, M.B. Braga, Chaos in shape memory two-bar truss, Int. J. Non-Linear Mech. 37 (1) (2002) 1387–1395.
[25] Z.Q. Wu, Z.H. Zhang, Force–displacement characteristics of simply supported beam laminated with shape memory alloys, Acta Mech. Sin. 27 (6) (2011) 1065–1070.
[26] X. Yan, J. Nie, Response of SMA superelastic systems under random excitation, J. Sound Vib. 238 (5) (2000) 893–901.
[27] G. Ge, Response of a shape memory alloy beam model under narrow band noise excitation, Math. Probl. Eng. 2014 (2014). 7 pages.

[28] M.I. Friswell, O. Bilgen, S.F. Ali, G. Litak, S. Adhikari, The effect of noise on the response of a vertical cantilever beam energy harvester, ZAMM (2014) 1–11.
[29] J.-C. Lee, J.-C. Chen, Active structural acoustic control for rectangular plate with a line moment excitation, J. Mech. 14 (2) (1998) 75–82.
[30] S. Assaf, M. Guerich, Numerical prediction of noise transmission loss through viscoelastically damped sandwich plates, J. Sandw. Struct. Mater. 10 (2008) 359–384.
[31] G. Ge, H. Wang, J. Xu, Stochastic bifurcation of rectangular thin plate vibration system subjected to axial inplane Gaussian white noise excitation, Trans. Tianjin Univ. 1 (2011) 13–23.
[32] J. Wiciak, Investigations of a noise control of a plate with four pairs of piezoelectric elements, Arch. Acoust. 31 (4) (2006) 503–512.
[33] A. Manela, Vibration and sound of an elastic wing actuated at its leading edge, J. Sound Vib. 331 (2012) 638–650.
[34] P.H. White, Sound transmission through a finite, closed, cylindrical shell, J. Acoust. Soc. Am. 40 (5) (1966) 1124–1130.
[35] C. Durant, G. Robert, P.J.T. Filippi, P.-O. Mattei, Vibroacoustic response of a thin cylindrical shell excited by a turbulent internal flow: comparison between numerical prediction and experimentation, J. Sound Vib. 229 (5) (2000) 1115–1155.
[36] F. Pellicano, Dynamic instability of a circular shell carrying a top mass under base excitation: experiments and theory, Int. J. Solids Struct. 48 (2011) 408–427.
[37] Karman Th., Festigkeitsprobleme in Maschinenbau, Encykl. D. Math. Wiss. 4 (4) (1910) 311–385.
[38] A.S. Volmir, Nonlinear Dynamics of Plates and Shells. Nauka, Moscow, 1972 (in Russian).
[39] J. Awrejcewicz, A.V. Krysko, V.A. Krysko, I.V. Papkova, Routes to chaos in continuous mechanical systems. Part 1: mathematical models and solution methods, Chaos Solitons Fractals 45 (2012) 687–708.
[40] J. Awrejcewicz, A.V. Krysko, V.A. Krysko, I.V. Papkova, Routes to chaos in continuous mechanical systems: Part 2. Modelling transitions from regular to chaotic dynamics, Chaos Solitons Fractals 45 (2012) 709–720.
[41] J. Awrejcewicz, A.V. Krysko, V.A. Krysko, I.V. Papkova, Routes to chaos in continuous mechanical systems. Part 3: The Lyapunov exponents, hyper, hyper-hyper and spatial-temporal chaos, Chaos Solitons Fractals 45 (2012) 721–736.
[42] J. Awrejcewicz, V.A. Krysko, I.V. Papkova, A.V. Krysko, Deterministic Chaos in One Dimensional Continuous Systems, World Scientific, Singapore, 2016.
[43] A. Wolf, J.B. Swift, H.L. Swinney, J.A. Vastano, Determining Lyapunov exponents from a time series, Phys. D. 16 (3) (1985) 285–317.
[44] M. Feigenbaum, Quantitative universality for a class of nonlinear transformations, J. Sat. Phys. 19 (1978) 25–52.
[45] M. Feigenbaum, The universal metric properties of nonlinear transformations, J. Stat. Phys. 21 (1979) 669–706.
[46] A.V. Krysko, J. Awrejcewicz, I.E. Kutepov, N.A. Zagniboroda, V. Dobriyan, V.A. Krysko, Chaotic dynamics of flexible Euler–Bernoulli beams, Chaos 34 (4) (2014) 043130-1–043130-25.